Experimental Investigation of a Wall Stabilized Arc With Comparisons to Theoretical Predictions

By

William Lee Wells

B. Sci. Tennessee Technological University, 1959

A Thesis submitted to the Faculty of the School of Engineering and Applied Science of the George Washington University in partial satisfaction of the requirements for the degree of Master of Science

June 1973

Abstract

A wall-stabilized, constricted-arc heater was investigated by extensive measurements of pressure, voltage, and wall heat flux at different axial locations along the constrictor. Radial temperature profiles were measured at one axial location by the radiance of a single line method and also by the continuum radiance at a wavelength of 4955 Å. The arc heater with an inside diameter of 2.37 cm and a constrictor length of 42 cm was operated with nitrogen flow rates from about 2 to 10 g/sec, and arc currents from 400 to 1200 amperes.

Based on a literature search, two different digital computer programs were selected which were used to predict the pertinent parameters by numerical solutions to the governing differential equations. The program selections were based on completeness and availability. In general the predictions were adequate when laminar flow was assumed, and the greatest difficulty was encountered in the predictions of wall heat flux.

The results of the measurements are shown in graphical form, along with the theoretical predictions from both computer programs.

ACKNOWLEDGEMENTS

The author wishes to thank Dr. Walter Olstad for his assistance in this study. A special thanks is offered also to Velvin Watson and Randolph Graves for making available computer programs used for the theoretical portion of this investigation, and to Walter L. Snow for his valuable advice and direction for spectrographic techniques.

The author is indebted to the National Aeronautics and Space Administration for permission to use material obtained from a research project at Langley Research Center in this thesis.

TABLE OF CONTENTS

LIST OF SYMBOLS

A	Einstein coefficient or transition probability
A	area
c	speed of light
C_p	specific heat at constant pressure
E	energy
E_z	axial voltage gradient
g	statistical weight
H	total enthalpy
$\bar{h}$	Planck's constant
h	static enthalpy
I	current
k	thermal conductivity
k	Boltzmann's constant
ℓ	pathlength
ℓ	mixing length in turbulent flow
$\dot{m}$	mass flow rate
N	radiance
N_{Pr}	Prandtl number
p	pressure
P	radiated power
q	heat input
Q	partition function
Q_w	wall heat flux

R gas constant

r radius

T temperature

u axial velocity

V voltage

v radial velocity

y distance from wall

Z compressibility factor

z axial distance from constrictor entrance

γ Stefan-Boltzman constant

ϵ turbulent eddy viscosity

λ wavelength

μ dynamic viscosity

$\bar{\mu}$ Planck mean absorption coefficient

ν kinematic viscosity

ρ density

σ electrical conductivity

τ shear stress

ϕ thermal conductivity function

Subscripts:

ℓ centerline

n upper energy state

nm from upper energy state to lower energy state

ref reference conditions

o constrictor entrance conditions

w wall conditions

LIST OF FIGURES

CHAPTER I

INTRODUCTION

The use of electric arcs to heat a gas to very high temperatures of order 10^4 degrees K has been a subject of scientific study for a number of decades. However, it has been within the last two decades that researchers have exploited this efficient and continuous source of energy for wide-scale, practical engineering use. Devices designed for this purpose are variously referred to as plasma jets, plasma torches, plasma generators, arc heaters, and arc jets. The search for an efficient and reliable energy conversion process as well as the particular intended application has resulted in several different designs for these devices. Representative of the applications are materials testing, spacecraft entry research, propulsion, flame spraying and coating, chemical synthesis, and radiation sources. A classification of the devices and their applications are discussed in reference 1.

Although devices of a number of different designs exist, they all have in common the requirement to control and contain the arc and gas in such a manner as to transfer the electrical energy of the system into the gas. One such device that is currently in common use is generally referred to as the wall-stabilized, constricted tube arc. In this configuration a cylindrical tube is employed with an electrode situated at each end so as to provide a direct-current arc along the tube axis and allow the flow of a gas co-axially with the

tube and arc. It is within the tube, or "constrictor", where most of the energy conversion takes place. The efficient design of such a device, along with it's auxiliary equipment, requires a knowledge of the results of the complex energy exchange processes that take place within the tube. Furthermore, intelligent utilization of these devices also depend upon a knowledge of the arc-gas interactions. In some instances it is sufficient to know the aerothermodynamic state of the effluent gas as, for example, in some materials studies where samples are exposed to the heated gas stream. In other cases the complete spatial distribution of gasdynamic, thermal, and electromagnetic variables throughout the tube may be required. A most recent example of this latter case is a facility as reported in reference 2 wherein the gas throughout the constrictor is treated as a streamtube in the flow field behind the bow shock of a spacecraft during a simulated planetary entry.

Many investigators have performed theoretical analyses of the interaction between the electrical discharge and the gas flow within the constrictor. However, the energy exchange processes which take place within the tube are complex and consequently a number of simplifications and assumptions have been made in order to arrive at a tractable set of governing equations. The most successful efforts to date are those imploying numerical techniques which describe the gasdynamic, thermal, and electromagnetic variables in the constrictor inlet region as well as in the region of fully developed flow. One investigator (ref. 3) used numerical methods to solve the governing

equations to obtain wall parameters such as Nusselt number and friction factors in the fully developed flow region of the constrictor, however, instabilities were encountered at arc currents greater than 300 amps and/or gas flow rates greater than 3g/sec. An extensive review of the different theoretical models and their shortcomings have been covered in references 4 and 5, therefore no effort will be made here to evaluate the relative merits of each approach. However, as pointed out by Bower (ref. 3) in 1968, the most complete solution of the coupled system of conservation equations to date, was that due to Stine, Watson, and Shepard (ref. 6) and later published in detail by Watson and Pegot (ref. 7). More recently, a similarly complete approach was taken by Graves, but with a different, numerical technique as reported in reference 8.

In any case, the amount of published experimental verification is scanty and the range of reported arc current and gas flow rates are very limited. In some instances where data are available, insufficient information is presented to determine the conditions under which the measurements were made. In other cases only one or two parameters were measured. As pointed out in reference (4) a consistent set of experimental data is needed for the verification of the latest theoretical predictions of the flow field in a wall-stabilized constricted arc heater. Because of their relative completeness, availability, and suitability for digital computer computation the two latter mentioned approaches to a theoretical solution (ref. 7 and ref. 8) were selected for presentation with the present experimental

measurements. The experiment was run with nitrogen as the test gas and measurements were made at representative values of gas flow rates, arc currents, and stagnation pressures available with the present system. The programs were written in Fortran IV code[1] and executed by a CDC 6600 digital computer. For each experimental test both programs were run with the same values of input gas mass flow rate, entrance pressure, and arc current.

---

[1]The program of reference 7 was received written in Fortran II code but was changed to Fortran IV.

CHAPTER II

THEORY

The approach taken by the two selected sources, (ref. 7 & 8) to analytically describe the plasma flow in a constricted tube arc is from a macroscopic point of view. The macroscopic model treats the plasma as a homogeneous, isotropic continuum which satisfies the classical system of fluid mechanic equations combined with the necessary electrodynamic relations. The fluid mechanic equations are based on the conservation of mass, momentum, and energy in some arbitrary control volume within the flowing plasma. The complete set of electrodynamic relations include Ohm's law, Maxwell's equations, and the linear constitutive field equations, of which the latter two relate the electric and magnetic fields. Since no externally applied magnetic field is utilized in the constricted tube arc, most of the electrodynamic effects have been considered insignificant by these two papers, and only the portion of Ohm's law which relates current to the electric field and the electrical conductivity has been retained. However, electromagnetic effects which appear in the energy equation as a Joule heating term have been retained. Consideration of the full electromagnetic effects would have resulted in additional terms in the momentum eq. in the form of Lorentz body forces, but the continuity eq. would have been unaffected. The rationale for exclusion of most of the electrodynamic effects is discussed at some length in reference 3. In addition to the previously mentioned

equations, the thermodynamic relations must also be satisfied. The thermal equation of state relates the pressure, temperature, and chemical composition; $\frac{p}{\rho} = ZRT$ where Z is an indication of the degree of dissociation and ionization. The caloric equation defines the enthalpy in terms of the constant-pressure specific heat; $h-h_{ref} = \int_{T_{ref}}^{T} c_p dt$. Finally, it is necessary to specify the functional dependence on temperature of the thermodynamic and transport properties and the appropriate boundary conditions for the flow field.

After the governing equations have been somewhat simplified by the restriction of the electromagnetic effects, there still remains a highly complex, interlated system of non-linear partial differential equations. A number of approximations, and simplifications have been made in both analyses in order to make the system of equations more amenable to a solution. These assumptions and simplifications are listed below.

1. The gas flow is steady and axisymmetric.
2. The electric discharge is stationary and the electric potential is constant on planes perpendicular to the axis.
3. Axial heat conduction is negligible compared to radial heat conduction.
4. Lorentz forces are negligible compared to dynamic and static pressure forces.
5. The radial pressure gradient is negligible compared to the static pressure.

6. The gas is assumed to be in local thermodynamic equilibrium.

7. The gas is optically transparent to all thermal radiation.

The form of the simplified governing equations from each of the two sources are listed below in a cylindrical coordinate system.

Reference 8

Continuity,

$$\frac{\partial}{\partial Z}(\rho u) + \frac{1}{r}\frac{\partial}{\partial r}(\rho v r) = 0 \qquad (1)$$

Momentum,

$$\rho u \frac{\partial u}{\partial Z} + \rho v \frac{\partial u}{\partial r} = -\frac{dp}{dZ} + \frac{1}{r}\frac{\partial}{\partial r}\left(r\mu \frac{\partial u}{\partial r}\right) \qquad (2)$$

Energy,

$$\rho u \frac{\partial H}{\partial Z} + \rho v \frac{\partial H}{\partial r} = \frac{1}{r}\frac{\partial}{\partial r}\left(r \frac{k}{C_p}\left[\frac{\partial H}{\partial r} + (N_{Pr} - 1)u \frac{\partial u}{\partial r}\right]\right) + \sigma E_Z^2 - P \qquad (3)$$

where $\sigma E_Z^2 = \dfrac{\sigma I^2}{\left[\int_0^{r_w} 2\pi r \sigma \, dr\right]^2}$ = the joule heating and where

$P = 4\bar{\mu}_p \gamma T^4$ = the radiated power.

Ohm's law,

$$I = 2\pi E_Z \int_0^{r_w} \sigma r \, dr \qquad (4)$$

The following boundary conditions are applied:

at the centerline, $r = 0$, $\frac{du}{dr} = 0$, $\frac{dH}{dr} = 0$

at the wall, $r = r_w$, $v = 0$, $u = 0$, $H = H_w$

Reference 7

Continuity,

$$\int_A \rho u dA = \dot{m} \tag{5}$$

Momentum,

$$\rho u \frac{\partial u}{\partial Z} + \rho v \frac{\partial u}{\partial r} = - \frac{dp}{dZ} + \frac{1}{r} \frac{\partial}{\partial r} (r\mu \frac{\partial u}{\partial r}) \tag{6}$$

Energy,

$$\rho u \frac{\partial H}{\partial Z} + \rho v \frac{\partial H}{\partial r} = \frac{I^2 \sigma}{(\int_A \sigma dA)^2} + \frac{1}{r} \frac{\partial \phi}{\partial r} + \frac{\partial^2 \phi}{\partial r^2} - \text{radiation} \tag{7}$$

where $\phi = \int_{T_{ref}}^{T} k dT$ = conductivity function, a mathematical device sometimes employed to reduce the number of unknown coefficients in differential equations of heat transfer theory.

In this investigation the measured values of pressure ranged

from about 0.1 to 1.0 atm. The program of ref. 7 utilizes the thermodynamic and transport properties of nitrogen, except for gas radiance, where the values for air were used. However, the variation of many of these properties with pressure were extrapolated into the range of interest here. The program of reference 8 was set up to utilize the property of air (without extrapolation). In reference 14 graphical comparisons are made for some of the properties of air and nitrogen. Where feasible other properties were compared at one atmosphere pressure by the present author. For the temperature of interest no significant differences were apparent except at occasional maxima values in a narrow temperature band. In general the differences even at these points were within the accuracy to which transport properties are known. Therefore, the programs were run with the "as received" property values with the realization that some differences in predictions may result from differences in property values. The sources of property values for each program are shown in Table I.

TABLE I

Property	Reference 7		Reference 8
h	$0 < h < 7 \times 10^7$	$7 \times 10^7 < h < 23 \times 10^7$	all
μ	ref. 15	ref. 16	ref. 17
k	ref. 15	ref. 18	ref. 17
c_p,h,Z	——	——	ref. 17
$\bar{\mu}_p$	——	——	ref. 19
σ	ref. 18	ref. 18	ref. 20
radiation	ref. 15	ref. 18	——

In the numerical approach a set of conditions are assumed at the constrictor entrance and through the governing equations a new set of conditions are calculated at a point a small distance downstream. An iterative process of calculating the new conditions is followed at the new axial station until the integral of the local mass flow over the cross-sectional area matches the total input mass flow to within a specified accuracy. This stepping procedure is followed throughout the constrictor length, where the conditions at each new step are determined from the previous step through consideration of mass, momentum, and energy. Near the entrance where conditions change rapidly, the distance between axial locations (step size) is small, and become progressively larger downstream. At each axial station the conditions are calculated at a number of discrete radial locations called mesh points sufficient to maintain numerical stability and provide accurate property profiles. The program of reference 7 has the radial mesh points evenly spaced between the constrictor centerline and the wall, whereas, ref. 8 spaces the points according to a geometric progression which results in a higher concentration of points near the wall where large changes in variables take place.

Reference 7 uses a fully explicit numerical technique whereas reference 8 uses an iterative implicit finite-difference technique. The primary difference being that the latter method determines new gas properties at each new axial station after the new enthalpy profile is estimated by use of the energy equation, but before proceeding to the momentum and continuity equations. In contrast, the

explicit technique makes use of gas properties from the previous step to determine the new profiles. Reportedly (ref. 3) the implicit method is more stable.

CHAPTER III

EXPERIMENTAL APPARATUS

Arc Heater System

The arc heater (see figure 1(a)) was of the wall stabilized type which utilized a constant diameter constrictor for stabilization and confinement of the arc and gas. The constrictor was 42.4 cm. long and 2.37 cm. inside diameter. The arc attached to a hollow tungsten cathode at the upstream end and to multiple (32) cooled copper anodes in a conical expansion section just downstream of the constrictor exit. The anodes were arranged in a radial configuration with sixteen in each of two rows. Resistors were in series with the anodes to cause the electrical current to divide evenly to each anode thereby resulting in a very quiescent arc. The constrictor was constructed of alternate wafers of ceramic insulators (boron nitride) and water-cooled heat conductors (copper) as shown in figure 1(b). Water lines to these wafers were nonconductive so that each wafer was electrically isolated and was allowed to rise to the local arc potential during operation. Six of the cooled wafers, or segments with a special configuration were spaced along the constrictor. Each of these segments contained a pressure orifice, a voltage connection, and was equipped with an individual water flow meter and a set of thermocouples for wall heat flux measurements. Another special segment contained two parallel cooling water passages with a solid land between them where a slot was cut through the wall to provide an

external view of one arc for temperature measurements. The slot height was equal and tangent to the constrictor inside diameter and had a width of 2.06 mm. The slot was covered and sealed by a quartz window on the outside of the arc heater. A cross section sketch of this special segment is shown in figure 1(c).

Shown in figure 2 is a view of the overall system where the primary components are; the arc heater, the vacuum system, the high pressure cooling water system, and an 1100 volt power supply. The exit of the arc heater was connected and sealed to a vacuum tank (of approximately 0.368 m^3) but was electrically isolated from it. Within the vacuum tank a cylindrical blunt body was situated near the exit and coaxially with the arc heater. Consequently the effluent gas was forced to turn and flow radially through the gap formed by the arc heater exit and the blunt body. The gap width was adjustable by movement of the blunt body through a remotely operated drive mechanism, thereby providing a means for pressure control in the arc heater at a fixed flow rate. The vacuum tank was connected to a 2,265 m^3 vacuum reservoir which was evacuated with pumps and blowers. Cooling water was supplied from a 227 m^3 reservoir through a high pressure pump, and nitrogen of 99.99 per cent minimum purity was supplied from storage cylinders.

The power supply consisted of two 1100-volt ac/dc silicon diode rectifiers in parallel. Adjustable circuit resistors were provided for current control.

Instrumentation

All of the data were taken in the form of continuous electrical signals and stored on magnetic tape at the rate of 400 samples per second. The nitrogen flow rate was measured with a calibrated choked flow nozzle, pressure data were taken with calibrated strain-gage transducers, and iron-constantan thermocouples were used to measure the temperature of inlet nitrogen and cooling water. The cooling water flow rates were measured with calibrated turbine flow meters. The arc current was measured by use of a shunt and a current transductor which is a device designed for electrical circuits that operate above ground potential. The voltages were measured with a voltage transductor, also for ungrounded circuits. The current and voltage measuring circuits were each calibrated as a unit. The circuit used for voltage measurement at the various axial stations is shown schematically in figure 3. Included in this circuit was a rotary stepping switch which allowed automatic sampling of the voltage at each station on command from a remote location.

To determine the radial temperature profile of the gas within the arc heater a 3.4 m Ebert spectrograph was employed to expose a photographic plate to the light radiated by the arc column. The photographic plate was Eastman Kodak Company's "spectral analysis no. 3."

The spectrograph has a movable grating which allows the selection of a desired wavelength at which the light intensity is to be measured. A sketch of the optical arrangement is shown in figure 4.

The optical train consists of the spectrograph, a lens, an aperture, a pivot mounted mirror, and the arc (or in the case of film calibration, a calibrated tungsten lamp). The mirror could be pivoted to project the light from either the arc or the tungsten lamp into the spectrograph. The aperture was selected to control the energy throughput , the degree of parallelism of the light, and the depth of field. Aperture selection for these purposes are discussed in reference 9.

On the basis of calibrations and data-reduction techniques, the estimated accuracy of the measured data is as follows:

Voltage	±3 percent
Pressure	±2 percent
Wall heat flux	±5 percent
Temperature	±10 per

CHAPTER IV

TEST PROCEDURES AND METHODS

Special Calibrations

Although all of the instrumentation was laboratory calibrated, special calibrations were also made at the site for the assembled measuring arrangements. As mentioned earlier, the [illegible]ete current and voltage circuits were calibrated with known inputs at the site. Periodically, the arc heater was pumped to various known pressure levels thereby exposing all pressure transducers at the different axial locations to a given pressure simultaneously. The output from the transducers were then compared to guard against possible connector leaks and changes in transducer calibrations.

The wall heat flux was determined by measuring the heat input to a cooled segment and dividing the numerical result by the exposed wall area. The wall area also includes one uncooled insulator segment since it is dependent upon the cooled segment for cooling. The heat input was determined by the cooling water flow rate and it's temperature rise through the control segment according to the relation;

$$q = \dot{m} C_p \Delta T \qquad (8)$$

To establish confidence in this combination measurement of flow rate and temperature rise a special calibration was devised. As sketched in figure 5 the cooled control segment was replaced by a length of

nichrome resistance ribbon enclosed in the flow passage of a 0.483 cm inside diameter nylon tube. A direct-current power supply was connected across the ribbon of known resistance thereby providing a precisely known input from the Joule heating. Heat inputs equivalent to a range of expected heat flux values were employed. The maximum deviation of the water flow/temperature rise derived heat output from the electrical input was 5 percent.

For each radial temperature profile measurement one photographic plate was used. The information recorded on each plate and it's respective purpose is listed below:

1. Arc column intensity measurements; from 4915 Å-NI line and 4935 Å-NI line radiation superimposed on continuum radiation with a wavelength range from about 4730 Å to about 5180 Å.
2. Continuum radiation of known intensity from a tungsten lamp to provide a relation between input intensity and photographic plate density.
3. Step filtered intensity input for relative effects of varying the intensity on the plate.
4. Unfiltered intensity to assure uniformity of input to step filters indicated in (3) above.
5. Mercury line radiation from a microwave discharge to provide an accurate wavelength location and to assure the reproducability of a known line shape.

There are a number of methods whereby the intensity of line radiation can be used to determine a gas temperature (ref. 10). The

method used here was that whereby a temperature is related to the absolute radiance of a single atomic line. The emission results from the transition of an orbital electron from one energy state, n to a lower state, m. In an isothermal gas slab the measured integrated radiance N_{nm} is related to the temperature T by the expression (ref. 10);

$$N_{nm} = \frac{hc}{4\pi} \ell\rho \frac{g_n}{Q} \frac{A_{nm}}{\lambda_{nm}} \exp. (-E_n/kT) \qquad (9)$$

where for a given wavelength λ_{nm} and pathlength ℓ the remaining quantities are either constants or are tabulated values that are a function of temperature and pressure. Since some of the quantities are functions of temperature, an iterative process is required to match the correct N_{nm} and T. In the present case a radial temperature profile of the cylindrical gas column is required, whereas, measurements of radiance can only be obtained from a side or lateral view. However, the cylinder can be considered to be broken up into thin isothermal concentric annular zones and a mathematical technique referred to as an "Abel integral inversion" applied to convert the measured lateral radiance to radial radiance per unit depth, commonly called the emission coefficient. Inherent in this method is the assumption of optical transparency, local thermodynamic equilibrium, and cylindrical symmetry.

In reference 11 Morris, et al derived a method whereby the gas temperature could be deter. ed by measurement of the continuum

radiation at a wavelength of 4955 Å. The continuum radiation was assumed to result from two mechanisms for which the temperature dependence of the radiance was theoretically known. Based on this assumption and measurements of 4955 Å continuum radiation at 1 and 2 atms pressure and at temperatures from 9000 to 14,000 ^{o}K, a table of temperature as a function of radiance was set up for pressures between 0.1 and 5.0 atm. The advantage of this method over the line method is the reduction in time and effort required to determine the temperature.

In the present experiment the use of photographic film for radiance measurements allowed a simultaneous measurement of the 4955 Å continuum and the line data, hence the continuum method was also used and the results compared with the line derived temperatures.

The preceding methods, especially adapted to photographic techniques, are discussed in considerable detail in reference 9.

Tests

The procedure for running an experimental test consisted of a pre-run instrument check, safety checks, and the actual arc heater operation. For the arc heater operation, the heater and vacuum tank were evacuated to a pressure of approximately 267 N/m^2 (2 mm-Hg), a small flow of argon gas was introduced into the arc heater, and the 1100 volts of the power supply was impressed across the electrodes. In this strong electric field and low pressure the argon ionized sufficiently to create a conductive path between the electrodes at which time the nitrogen flow was initiated and the argon flow was

stopped. After arc ignition the nitrogen flow rate was adjusted to the desired value and the gap at the heater exit was adjusted to assure sonic flow at the exit rather than within the arc heater. When an equilibrium operating condition was attained all of the data were taken.

Prior to the test, resistance in the power circuit was adjusted to produce the approximate desired current.

CHAPTER V

RESULTS AND DISCUSSION

The experimental tests were made with three different levels of arc current, and three different levels of gas flow rate at each of these operating conditions. The nominal values of current were; 400, 800, and 1200 amperes, and nominal flow rates were 2, 6, and 10 gms/sec. (In some instances the 6 gms/sec case was replaced with a 4.8 g/sec case in order to utilize the facility for certain other on going research.) For each experimental case the computer programs from both reference 7 and reference 8 were run with an input current, mass flow rate, and entrance pressure equal to that obtained in the experiment. In each case, each computer program was run in the laminar flow mode and also in the turbulent flow mode.

The results of both numerical computations for laminar and turbulent flow are compared to the experimental data in figures 7 through 8. Except for the radial temperature profile these figures show the value of the measured or computed parameter by the ordinate as a function of the axial location on the abyscissa. The radial temperature profile is shown for one axial location only and that is at 16.3 cm. Zero axial distance is considered to be the constrictor entrance and just downstream of the cathode surface. Magnetic effects may become significant within a few mean-free-paths of the cathode surface and are not taken into account in the computations. Since the pressure was not measured at the entrance, the first three

measured data points were graphically extrapolated back to the zero axial distance in order to obtain an input pressure for the computer programs. Throughout these figures the solid curve represents the computed values resulting from use of the program of reference 8, and the dashed curve represents computed values resulting from use of the program reported in reference 7. For brevity, in the remainder of this discussion the names of the first authors will be used instead of reference 7 and reference 8; Watson and Graves respectively. The measured data are shown as discrete points enclosed by a circle and have no curve associated with them. When one of the computed curves stop short of an axial distance of 41 cm the program has computed an axial centerline velocity equal to the local acoustic velocity (Mach number = 1). When this condition is computed the program will not proceed.[1]

400 Ampere Case

Pressure - Figure 6(a) shows the axial pressure at the lowest current levels and for the three different mass flow rates which increase from the bottom toward the top of the figure. The measured pressure drop is nearly linear with axial distance and is essentially constant at the two lowest flow rates. For the laminar case both programs predict the correct trend and only slightly under predict the pressure except near the end of the constrictor where the gradient is greater than the

---

[1]Reference 7 also reports a subroutine for continuation at supersonic velocity provided the cross sectional flow area is made to increase downstream of the sonic point.

experiment indicates. Note that both programs indicate sonic velocity in the constrictor at the highest flow rate but only Graves predicts sonic velocity at the lowest flow rate. During the test the pressure at station - 1 (Z = 5.2 cm) was monitored and the blunt body moved toward the heater exit until the pressure at station - 1 began to respond, thus indicating sonic flow in the gap between the exit and blunt body rather than in the constrictor. Obviously, the turbulent models are inappropriate for these conditions, for the values are vastly underpredicted and sonic velocity is reached much nearer the entrance than was indicated even by the laminar flow model. The turbulent predictions are more nearly in agreement with the laminar flow predictions and the measured data when the gas flow rate is small.

Voltage - For similar arc currents and gas mass flow rates the voltage is plotted in figure 6(b). The voltage at any axial location increases with flow rate and entrance pressure, and both laminar flow computations predict this trend. The slope of the predicted curves are flatter than the experimental data indicate, and is more obvious with increased flow rate. Numerically, the programs nearly agree with each other and disagree with the experiment by only about 13 percent at most, and this occurs near the constrictor exit at the highest flow rate. Again, as for the pressure data, the turbulent models neither agree with each other or with the experimental data. (At the lowest flow rate case Watson's turbulent prediction does agree with experiment, but this is probably fortuitous since none of the other parameters

corroborate it.)

Wall heat flux - In figure 6(c) the experimental data indicates that the wall heat flux quickly rises to a certain value near the constrictor entrance and remains nearly constant throughout the constrictor. The magnitude of the wall heat flux increases with flow rate and pressure. Graves' (reference 8) laminar model closely predicts the magnitudes and the trends with flow rate, but the turbulent flow predictions are nearly one-hundred per cent in disagreement, or else indicates early sonic flow. Both of Watson's (reference 7) predictions, laminar and turbulent, are in large disagreement with the experimental data.

Temperature - The radial temperature profiles for this current level (400 amperes) are shown in figure 6(d). In general the experimental profiles based on both NI lines and the continuum are in good agreement and the profile becomes slightly more peaked at the centerline as the mass flow rate increases. At the highest flow rate the irregular continuum derived profile possibly results from an experimental error, although it must be recalled that this method was originally based on measurements at 1 and 2 atm. (reference 11). The measurements indicate a centerline temperature from about 11,500 K to about 13,000 K and the highest centerline temperatures occur with the highest flow rates. The tendency of the temperature to level out at large radii may result from the shape of the window slot which could allow a bulge in the flow at that point. Although the slot width is narrow, some hot gas

could conceivably flow in and out of it thereby disturbing the symmetry of the observed hot flow which is important to the temperature measurement technique as previously discussed. Both laminar flow solutions are in very good agreement with the data at least over the inner 50 per cent of the radius. Graves turbulent flow model predicts a considerably flatter profile than does the laminar flow model, which would be expected based on ordinary pipe flow. No turbulent predictions are shown in the highest flow rate plot because both programs predicted sonic flow prior to this axial station ($z = 16.3$ cm).

The variations in the calculated curves near 7000 K result from gas property variations rather than any numerical instabilities.

800 Ampere Case

Pressure - The axial pressure drop for this arc current case is shown for the three flow rates in figure 7(a). The experimental data indicates an almost linear drop with axial distance and linearity is enhanced by lowering the flow rate. Graves' laminar flow prediction is the most successful and Watson's laminar flow is next. In some instances sonic flow is predicted in the constrictor and a relatively sharp drop in pressure usually preceeds a predicted sonic point. The experiment does not indicate such a drop. As in the previous case (figure 6) the turbulent models are very unsuccessful except in the lowest flow rate case where the turbulent and laminar predictions are virtually the same.

Voltage - The voltage for the 800 amp case is shown in figure 7(b). The experimental data indicate a larger gradient at this operating condition than for a comparable flow and pressure at 400 amps. Although in general both laminar flow predictions agree reasonably well with the data, it would be desirable to have the slopes (or gradients) in better agreement for possible future heater design purposes. That is, if a heater of greater axial length is desired the voltage requirements could be under predicted by the calculations.

Wall heat flux - The experimental data in figure 7(c) indicate that the wall heat flux is much greater for this current level than for the 400 amp case. There is some indication of a wall heat flux reduction near the end of the constrictor, possibly due to uncompensated radiative losses from the exit. Graves laminar flow model predicts the wall flux quite well except in the lowest flow rate case, where it over predicts near the entrance and underpredicts near the downstream end. Watson's laminar model predicts nearly the opposite to Graves in the lowest flow case and vastly underpredicts for the two higher flow rates. Neither of the turbulent models adequately describe the wall heat flux.

Temperature - The radial temperature profiles for this case are shown in figure 7(d). The centerline temperatures are not greatly different than those measured at 400 amps, but the profiles are slightly flatter indicating that the arc tends to more nearly fill the tube as the current is increased. Centerline temperatures for this case are from

about 13,000 to 14,000 K. Both laminar flow programs predict the profiles adequately, although Watson predicts a more peaked profile with increasing flow rate than is born out by the experimental data. Watson predicts a higher centerline temperature for the turbulent case, whereas Graves predicts a lower value.

1200 Ampere Case

Pressure and Voltage - For this case the axial pressure and voltage drop are shown in figures 8(a) and 8(b) respectively. The results, except for magnitudes, are very nearly the same as for the lower current cases.

Wall heat flux - In figure 8(c) the experimental data indicates a differ :t pattern of wall heat flux as the flow rate is increased. For the lowest flow rate the heat flux rises throughout the first half of the constrictor length and then approximately levels out in the last half. In the two larger flow rates the heat flux quickly rises to a value which is almost constant throughout the constrictor. In a crude sense, Graves predictions follow this latter pattern for all three flow rates. In the two larger flow rates Graves laminar flow computations approximate the magnitude of the flux levels also. Watson predicts the low flow rate case best, and following a very slow rise, appears to approach the correct value near the end of the constrictor for the middle flow rate. Watson's highest flow rate case predicts the correct pattern but the magnitude is underpredicted by nearly a factor of four, and the turbulent model is about as good as the

laminar model for all three flows. Graves turbulent model predicts lower wall heat fluxes than does the laminar model, which seems contrary to ordinary pipe flows with heat transfer. However, at the high temperatures involved the radiative heat flux componenet is important, so that if turbulent flow results in a much lower centerline temperature the net result may be a reduced wall heat flux.

Temperature - In figure 8(d) there is a greater difference between the line derived and continuum derived temperature profiles than was seen in the previous lower current, lower pressure cases. Here the continuum method indicates a peak temperature on the order of 10 per cent greater than the line method, although the best agreement would have been expected at this pressure near one atmosphere where the relation between continuum measurements and temperature were originally derived (see reference 11). Considering all of the temperature measurements however, the continuum method has compared very favorably with the line method which required much more time and effort. Both theoretical laminar flow computations indicate a much higher centerline temperature; approximately 16,000 K as compared to measured values on the order of 13,000 K. Graves turbulent case predicted sonic flow prior to this axial location, and Watson's turbulent values at the centerline are approximately 100 per cent higher than the measured values, and therefore again fail to predict the measured results.

Overall Considerations

Considering the over all results of figures 6 through 8, the most apparent results is that the turbulent mode of either program fails to predict the measured results. Based on the predictions it can only be concluded that the flow in each case is indeed laminar. In most cases however, the two turbulent results do not agree with each other, a clear indication that one, or both, methods are in error. The experimental data provides no insidht in this regard, however, a few observations may be made. In Graves' program, the change from the laminar mode to the turbulent mode results in the use of a turbulent Prandtl number (approx. unity) instead of a laminar Prandtl number (approx. 0.7) and the use of a turbulent coefficient of viscosity in the governing equations. The turbulent viscosity being the sum of the molecular viscosity and an apparent viscosity due to "lumps" of fluid with a fixed axial velocity and momentum that travel a transverse distance "ℓ" in the stream. This transverse (radial, in this case) distance "ℓ" is generally referred to as the "mixing length" and was first conceived by L. Prandtl in 1925. There are a number of different relations for the mixing length in the literature and the semi-empirical one used by Graves is referred to as the Van Driest model and is;

$$\ell = 0.4y \left[1 - \exp. \left(- \frac{y\sqrt{\tau_w \rho_c / \rho_w}}{26\, \nu_w} \right) \right] \qquad (10)$$

where y is the distance from the wall and the exponential term is evaluated at the wall properties (reference 12). When the

exponential term is expanded it becomes apparent that ℓ is proportional to y^2 at the wall and at centerline ℓ is approximately equal to 0.4 r_w, that is;

$$\ell \propto y^2 \quad \text{for} \quad y \to 0$$

$$\text{and} \quad \ell \approx 0.4\, r_w \quad \text{at} \quad y = r_w$$

Actually the exponential term can be deleted and $\ell = 0.4\, y$ for all y greater than about 0.05 cm. for the conditions of interest here. Watson's program follows a similar procedure except that the mixing length used was the wholly empirical relation;

$$\frac{\ell}{r_w} = 0.14 - 0.08\,(1 - y/r_w)^2 - 0.06\,(1 - y/r_w)^4 \tag{11}$$

due to Nikuradse (reference 13). Expansion of this relation indicates that $\ell_w \propto y$ and $\ell_{\mathcal{L}} \approx 0.14\, r_w$. It can be shown theoretically that

$$\lim_{y \to 0} \ell \to 0$$

and

$$\lim_{y \to 0} \frac{d\ell}{dy} \to 0 \text{ , (see reference 14 page 2-13).}$$

Equation 10 meets this criterion, however in equation 11 $\frac{d\ell}{dy} = 0.4$ at $y = 0$. Both equations 10 and 11 are plotted in figure 9.

In either case the apparent or "eddy" viscosity (ε) is related to the mixing length by;

$$\varepsilon = \ell^2 \left|\frac{du}{dy}\right| \tag{12}$$

Investigators (reference 12) who compared experimental, strongly heated gas flow data to several turbulent models concluded that the "Van Driest wall" model gave the best results of those tested.

Considering only the laminar flow results, Graves in most instances more accurately predicted the measured results. This was especially true of wall heat transfer and temperature. The measured wall heat flux exhibited two axial profiles. When the flow rate was small (2.2 g/sec) the heat flux tended to show a gradual rise from the entrance and then a leveling off trend toward the downstream end. For larger flow rates the measured heat flux tended to rise quickly near the entrance and maintain a nearly constant value throughout the constrictor. Watson's program portrayed this change in profile with flow rate, but the numerical values were usually greatly different from the measured values. Grave's profiles always exhibited the quick rise pattern near the entrance, but in general gave acceptable values. The total wall heat flux can be divided into two components; radiation, and conduction plus convection in both programs. One of the previously discussed laminar cases (see figure 7(c) , $\dot{m}$ = 4.8 g/sec) was replotted in terms of these components and is shown in figure 10. Both programs predict a radiative heat flux that exceeds

the convection plus conduction component in the entrance region and then predicts a decrease with axial distance. This seems reasonable since a cold gas is near the wall and the centerline temperature is high at the entrance. It can be seen from this plot that the difference in Graves' and Watson's axial heat flux profile is primarily due to the difference in the predicted radiative flux. Graves' radiative flux exceeds Watson's values by more than a factor of five, and the nearly constant total heat flux results from a decrease in radiation at about the same rate as the increase in conduction and convection with axial distance. The strean enthalpy near the constrictor exit is still sufficiently high enough to produce appreciable radiation in contrast to Watson's prediction in figure 10 (z = 38 cm.).

In reference 7, one of the chief advantages cited for Watson's program was the short computer run time required to get a solution. This was accomplished in part by minimizing the number of radial points where the numerical calculations are made. Watson's program has 13 radial mesh points, whereas Graves' program has 31. To check the effect of the number of radial mesh points the most expedient approach was to reduce Graves' radial mesh points to 13 also. A previous case was picked where good agreement with experiment was obtained and the case was re-run with the lower number of radial mesh points. These results are shown in figure 11. The measured results are shown for reference. Reducing the number of mesh points had a negligible effect on the pressure, voltage, and centerline temperature. The wall heat flux, however, was more sensitive to the change which

produced some instabilities in the program that resulted in oscillations in the solutions near the entrance region and also a reduction in magnitude by as much as 28 per cent near the exit. The quick rise feature near the entrance was not lost, however. Consequently, if temperature, pressure, or voltage are the properties of interest, significant reductions in computer time and cost can be achieved by reducing the number of radial mesh points. If accuracy in wall heat flux is desired then the number of mesh point should be increased.

In all of the results previously considered, both programs were run with an input static-enthalpy profile and axial-velocity profile at the entrance of the constrictor. The enthalpy profile can be described by the cubic equation;

$$H - H_w = (H_{\mathcal{L}} - H_w)\ (1.0 - 3R^2 + 2R^3) \quad \text{where} \quad R = \frac{r}{r_w} \ ;$$

and the velocity profile by the parabolic equation;

$u = u_{\mathcal{L}}\ (1.0 - R^2)$ where $u_{\mathcal{L}}$ is obtained from mass flow constraints. Actually, the inlet enthalpy and velocity profiles are unknown in the experiment, and the profile selections are arbitrary. To check the effect of changing these entrance profiles, one of the previously considered cases was re-run with different profiles that are more peaked at the centerline than the previous ones. The new and original profiles are shown in figure 12. The combinations of these profiles that were tried are:

1. peaked enthalpy/parabolic velocity
2. cubic enthalpy/parabolic velocity
3. peaked enthalpy/peaked velocity
4. cubic enthalpy/peaked velocity

Combination 2 will be recognized as the previously used combination. The results of these tests are shown in figure 13 for Watson and in figure 14 for Graves. The experimental data, is included for reference and the number assigned to each curve corresponds to the enthalpy/velocity profile combination listed above. Watson's program does not output temperature, but it does output enthalpy and a separate program had to be generated in order to get the previously shown temperature profiles. It was desirable to determine the effect of entrance profiles on parameters throughout the length of the constrictor and rather than convert the enthalpy at the numerous axial points with decreasing pressure, the centerline enthalpy was plotted instead of temperature.

From Watson's results in figure 13 it can be seen that the change in entrance velocity profile has very little overall effect on any of the parameters. (Compare combinations (1) and (3), and (2) and (4).) The effect of changing enthalpy profile is more pronounced. The effect on pressure, voltage, and wall heat flux persists throughout the length of the constrictor and the wall heat flux experiences the greatest effect. The peaked enthalpy profile best describes the experimental pressure and voltage whereas the cubic profile offers some improvement on the wall heat flux prediction. Very near the

entrance (within about 1/3 diameter) a vast difference in predicted centerline enthalpy exists for the two entrance enthalpy profiles. However, after approximately two diameters downstream the predictions are in good agreement. Experimental temperature measurements in the first cm. of length may shed some light on the correctness of the respective profiles, although the assumption of LTE on which the measurements are based may be questionable in this region near the cathode.

In order to get Graves' program to function with the sharp entrance enthalpy profile it was necessary to reduce the size of the axial steps taken between computations, and to increase the number of iterations to achieve convergence of the numerical solutions at a given axial station. The net result being an increase by a factor of two in computer time and cost. From figure 14 it can be seen that the change in entrance velocity profile has a negligible effect except for heat flux and enthalpy in the entrance region. When the entrance enthalpy profile was sharp the program had difficulty in converging on a solution for the wall heat flux in the entrance region however, these oscillations in the solution damped out after about two diameters downstream. Graves does not predict the very large peak in centerline enthalpy at the entrance that Watson does when the input enthalpy profile is peaked.

If approximately the first two diameters are discounted the effect of changing the input profiles as indicated here had no major effects on the results of either program, with the exception of Watson's wall heat flux prediction.

The intensity measurements used to determine the temperature by the line method can be used as an indication of the optical transparency of the gas at these wavelengths (4915 - 4935 Å). The radiation intensity results from the electronic transition from an upper energy state to a lower energy state. The lower state in this case actually consists of two levels and the resulting emission shows up as two lines, called a doublet, at 4915 and 4935 Å. The probability of electrons populating the two energy levels is a fixed ratio, and if the gas is thin the resulting emission intensities of the two lines will follow this same fixed ratio. Within the accuracy of the experiment this was found to be true, and is evidenced by the constant relationship between the two line determined temperatures in figures 6 through 8. Therefore the assumption of optical transparency for these wavelengths seems justified.

CHAPTER VI

CONCLUDING REMARKS

For the range of pressure, gas mass flow rates, and arc currents considered in this paper the following general concluding remarks are made.

The pressure decreases almost linearly with axial distance and the gradient increases with flow rate. The voltage increases almost linearly with axial distance and the gradient increases with flow rate and pressure. When the flow rate is small (about 2 g/sec) the wall heat flux has a tendency to rise slowly in the first half of the constrictor and level out in the downstream half. At larger flow rates (up to 10 g/sec) the heat flux quickly rises near the entrance to a nearly constant value throughout the constrictor. The wall heat flux is a strong function of current and pressure, e.g. at 400 amps and 0.58 atm the heat flux is about 150 W/cm^2, whereas at 1200 amps and 0.96 atm it is about 750 W/cm^2. Centerline temperatures varied from about 12,000 to 14,000 K and although the centerline temperature did not vary greatly with current, a larger portion of the stream was at a higher temperature for the higher currents. In a crude sense the radial temperature profiles were parabolic, and the profiles were more peaked with increased flow rate. In most cases the temperature derived from measurements of continuum radiation intensity at a wavelength of 4955 Å agreed with the temperature as derived from measurements of radiation intensity from the 4915 A NI line and also the 4935 Å line. The NI line derived

temperature is much more tedious to obtain than that from the continuum method, primarily because of the corrections which must be determined for the line shapes. The measured relative intensities of the 4915 Å and 4935 Å lines indicated that the gas was optically transparent at these wavelengths.

Both computer programs of reference 7 and reference 8, generally predicted the correct trends for the parameters and usually predicted the values to an acceptable accuracy when the laminar flow mode was used. The exception to this was the prediction for wall heat flux, where reference 7 failed to predict the values for most cases and the accuracy of reference 8 was not good at the highest current. At 1200 amps both programs overpredicted the centerline temperature by about 20 per cent. Reducing the number of radial mesh points, where the numerical calculations are made, by about 58% had little effect on the predictions except for wall heat flux. In general changing the input velocity and enthalpy profiles did not have a large effect on the predictions except within about two diameters of the entrance. In most cases the turbulent flow predictions of both programs did not agree with the measurements or with each other.

REFERENCES

1. Dennis, P. R., and Smith, C. R., Compilers; Gates, D. W., and Bond, J. B., ed.: "Plasma Jet Technology." NASA SP-5033, 1965.

2. Walberg, G. D., Wells, W. L., and Houghton, W. M.: "The Langley Planetary Entry Radiation Facility - Design Concept, Operational Characteristics, and Preliminary Test Results." A paper presented at the 37th Semiannual Meeting of the Supersonic Tunnels Association. May 4-5, 1972.

3. Bower, W. W.: "Correlations for the Wall Parameters in the asymptotic Region of a Laminar Constricted Arc.": M. S. Thesis, Purdue Univ., Jan. 1969.

4. Skifstad, J. G.: "Review of Theoretical Analysis of Arc Heating in a Tube." ARL 65-207, U. S. Air Force, October 1965.

5. Knabe, W. E.: Evaluation of Existing Literature on the Interaction of High - Density Plasma with Electric, Magnetic, and Fluid Dynamic Fields." ARL 64-34, February 1964.

6. Stine, H. A., Watson, V. R., and Shepard, C. E.: "Effect of Axial Flow on the Behavior of the Wall - Constricted Arc." AGARD - ograph 84, Part I, Arc Heaters and MHD Accelerators for Aerodynamic Purposes, 1964.

7. Watson, V. R., and Pegot, E. B.: "Numerical Calculations for the characteristics of a Gas Flowing Axially Through a Constricted Arc." NASA TN D-4042, 1967.

8. Graves, R. A., and Wells, W. L.: "Preliminary Study of a Wall Stabilized Constricted Arc." NASA TM X-2700, 1973.

9. Snow, W. L.: "Practical Considerations for Abel Inverting of Photographic Data with Application to the Analysis of a 15-kw Wall - Stabilized Arc - Light Source." NASA TN D-6672, 1972.

10. Tourin, R. H.: Spectroscopic Gas Temperature Measurement. Elsevier Publishing Co., Amsterdam, 1966.

11. Morris, J. C., Krey, R. U., and Bach, G. R.: "The Continuum Radiation of Oxygen and Nitrogen for use in Plasma Temperature Determination." J. Quant. Spectrosc. Radiat. Transfer, Vol. 6, pp. 727-740. Pergamon Press LTD., 1966.

12. Bankston, C. A., and McEligot, D. M.: "Turbulent and Laminar Heat Transfer to Gases with Varying Properties in the Entry Region of Circular Ducts." Int. J. Heat Mass Transfer. Vol. 13, pp. 319-344. Pergamon Press 1970.

13. Schlichting, H.: "Boundary Layer Theory." 4 th ed., pp. 508-514, McGraw - Hill, 1960.

14. Kendall, R. M., Rubesin, M. W., Dahm, T. J., Mendenhall, M. R.; "Mass, Momentum, and Heat Transfer Within a Turbulent Boundary Layer with Foreign Gas Mass Transfer at the Surface"; Office of Naval Research and Advanced Research Projects Agency, Wash. D. C. Feb. 1, 1964.

15. Ahtye, W. F., and Peng, Tzy - Cheng: "Approximations for the Thermodynamic and Transport Properties of High - Temperature Nitrogen." NASA TN D-1303, 1962.

16. Spitzer, L. Jr.: "Physics of Fully Ionized Gases." Interscience Publishers, Inc., New York, 1956.

17. Hansen, C. F.: "Approximations for Thermodynamic and Transport Properties of High - Temperature Air." NASA TR R-50, 1959.

18. Yos, J. M.: "Transport Properties of Nitrogen, Hydrogen, Oxygen, and Air to 30,000°k." Avco Corp., RAD-TM-63-7, 1963.

19. Landshoff, R. K. M., and Magee, J. L.: "Thermal Radiation Phenomena, Vol. 1, Radiative Properties of Air." IFI/Plenum, New York - Washington, 1969.

20. Arave, R. J.: "Approximate Thermodynamic, Transport and Electrical Properties of High - Temperature Air." Boeing Co. DZ-11781, 1963.

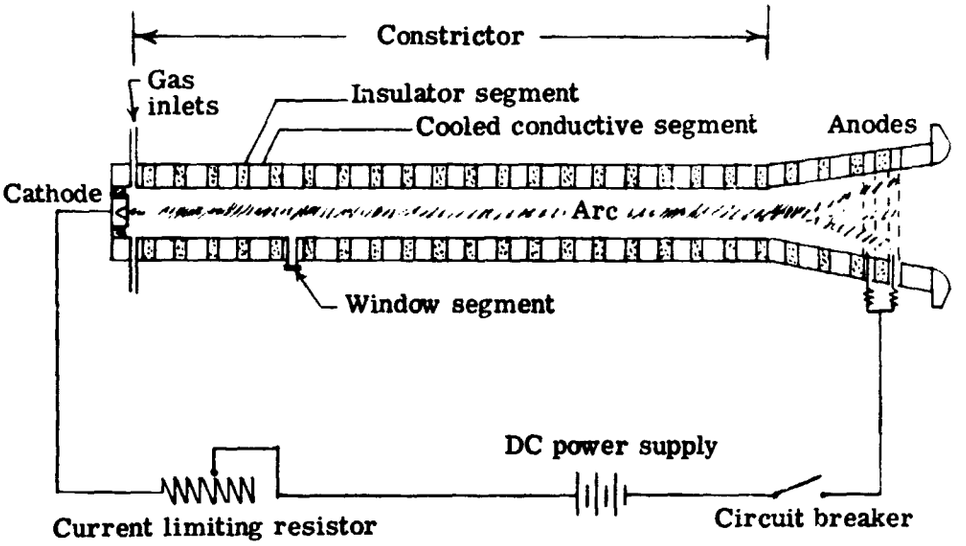

(a) Cross section of heater

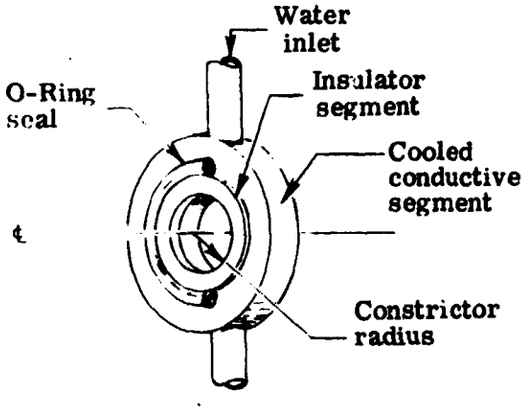

(b) Typical set of segments

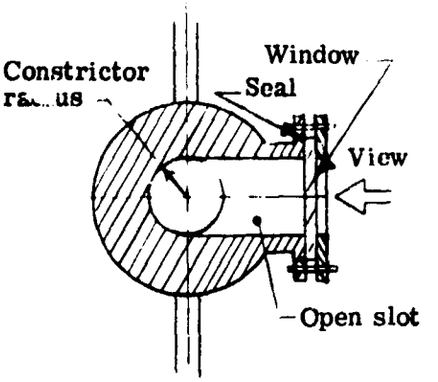

(c) Cross section sketch of special cooled segment with quartz window

Figure 1.- Schematic of arc heater and power circuit.

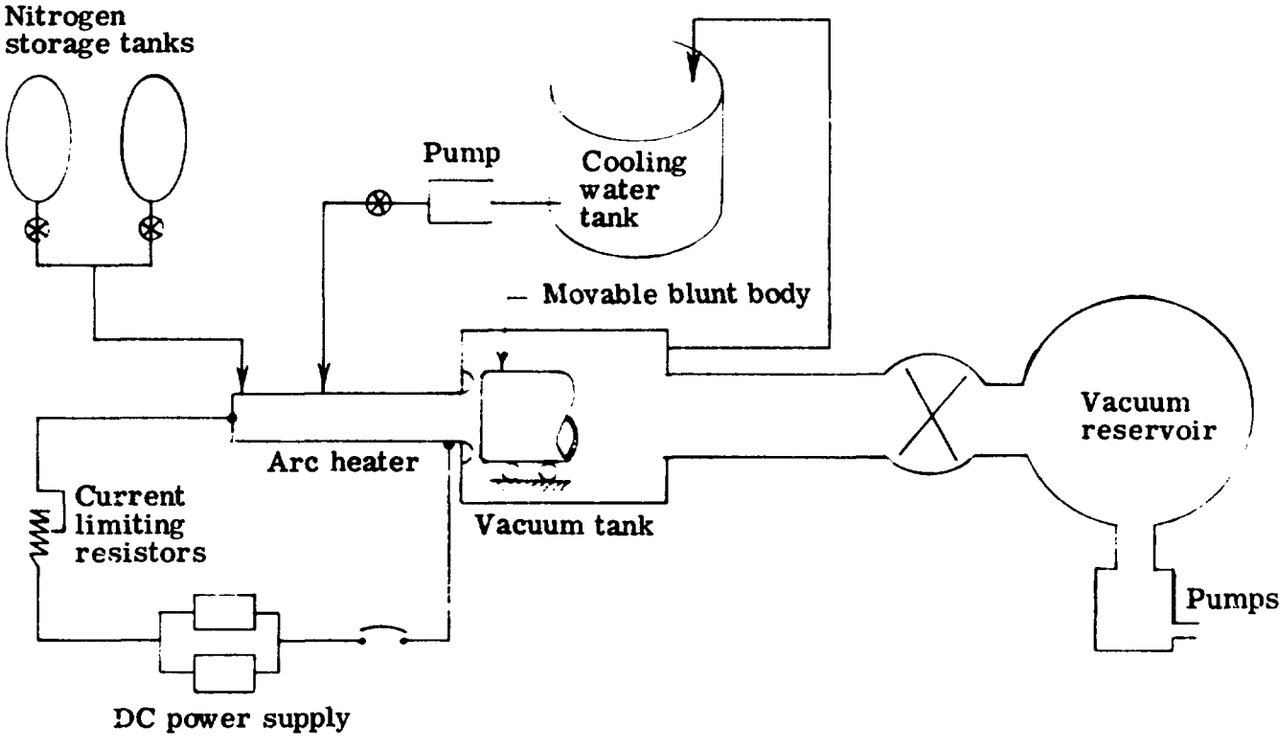

Figure 2.- Schematic of total experimental system.

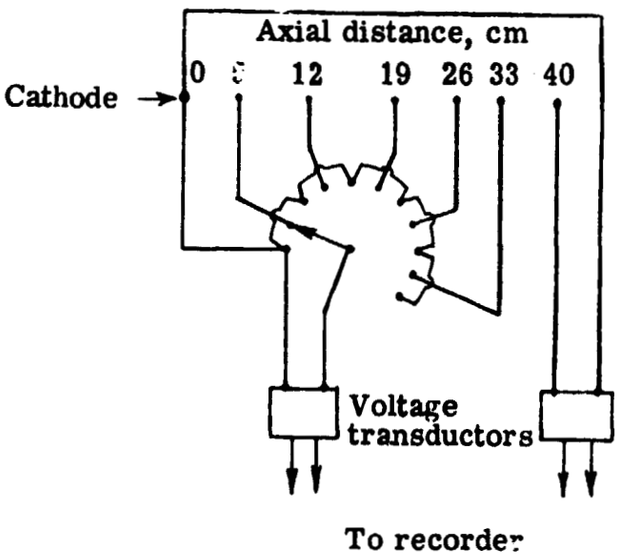

Figure 3.- Schematic of voltage measuring circuit.

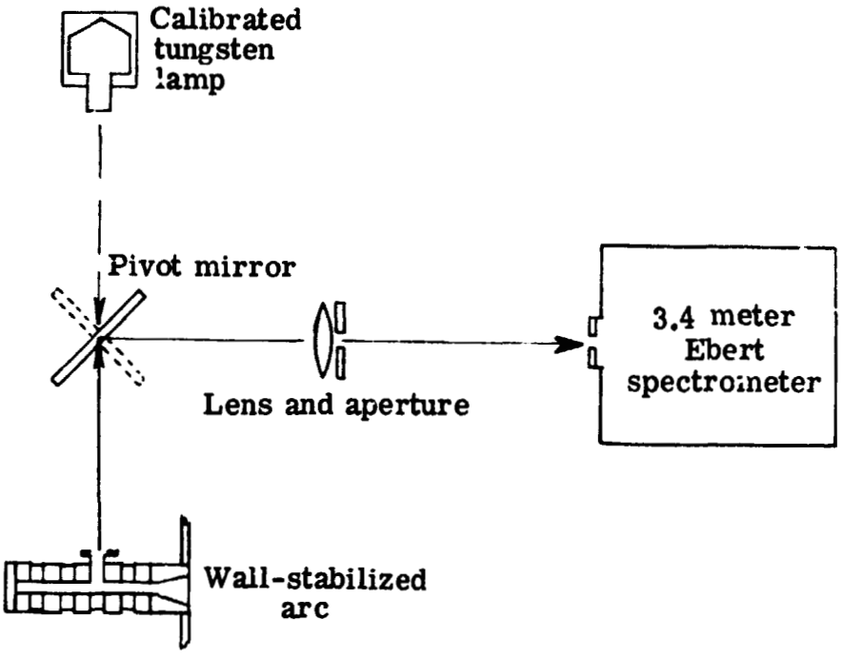

Figure 4.- Schematic of temperature measuring apparatus.

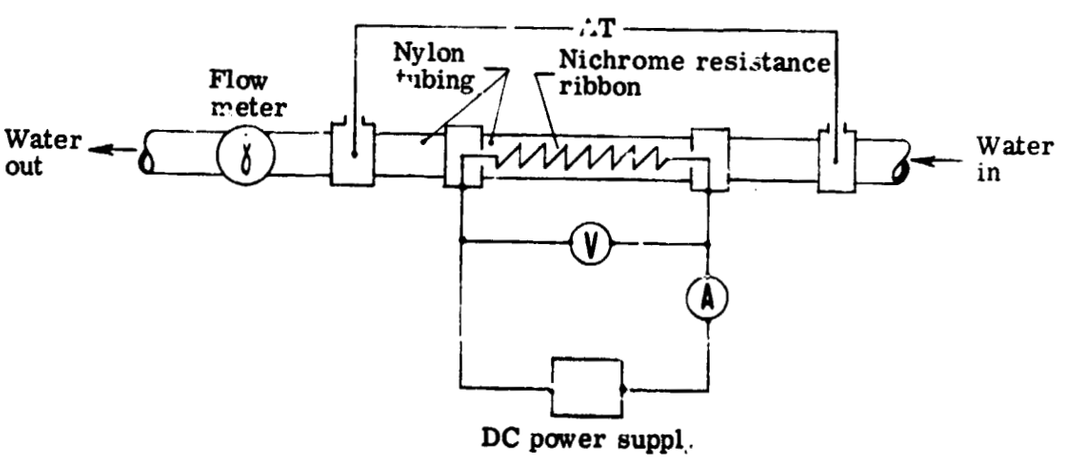

Figure 5.- Calibration arrangement for wall heat flux measuring apparatus.

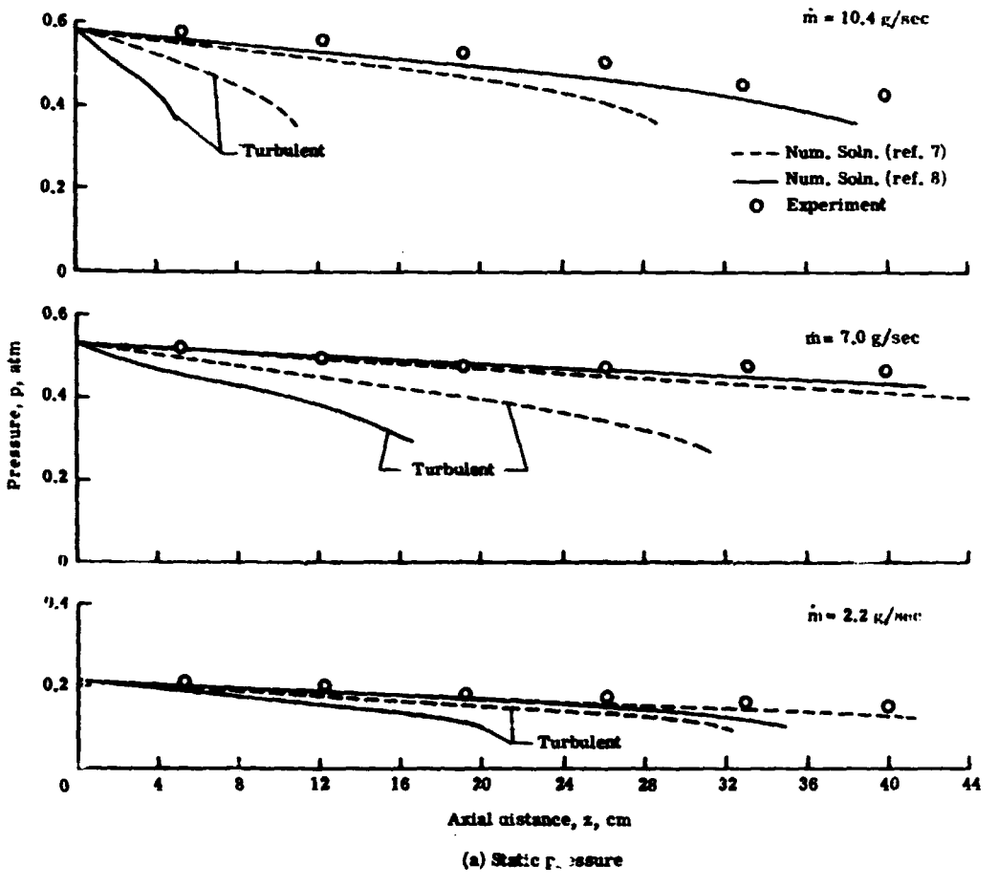

(a) Static pressure

Figure 6.- Variation of parameters with axial location in the constrictor for I = 400 amps.

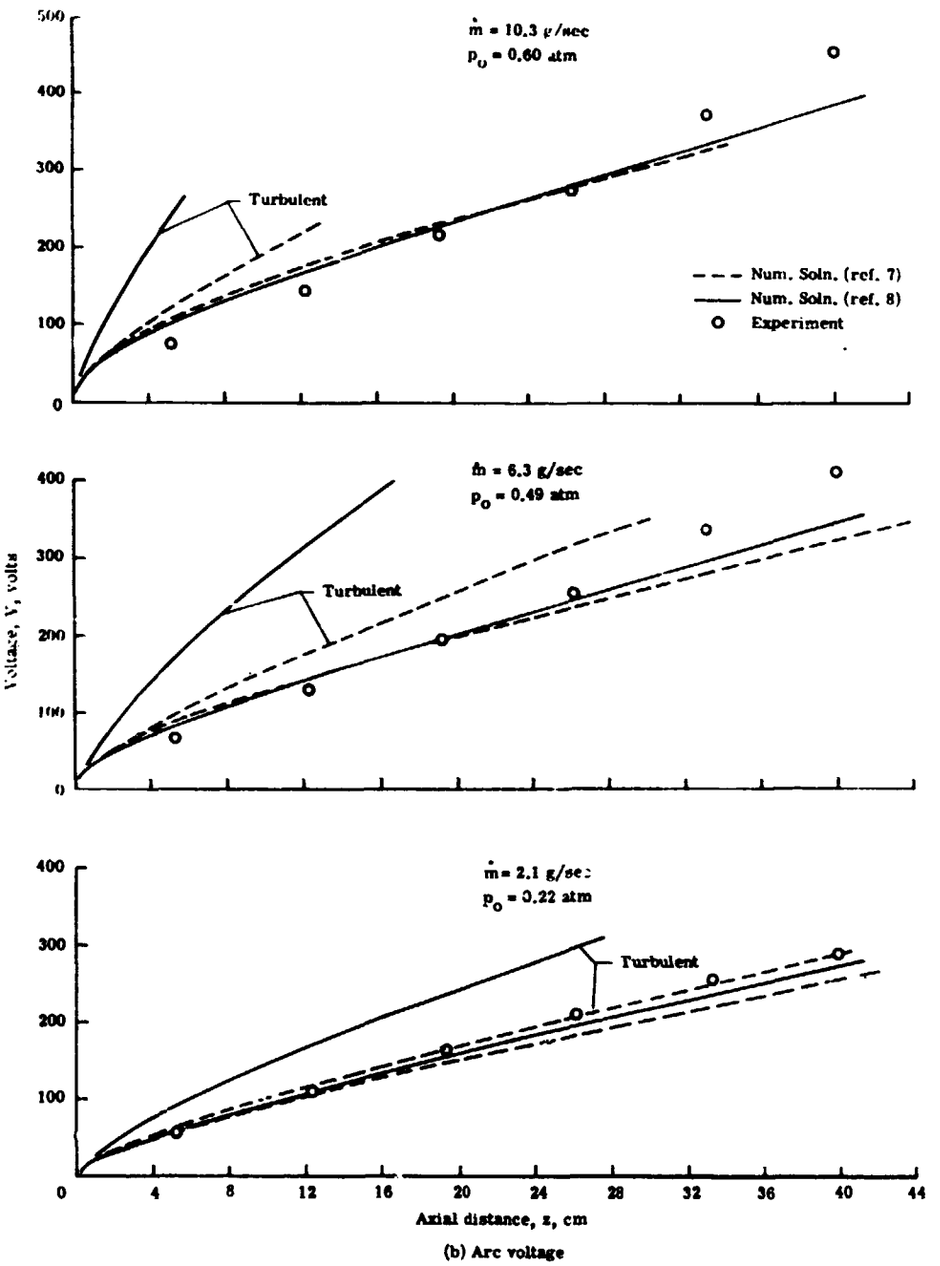

(b) Arc voltage

Figure 6.- Continued.

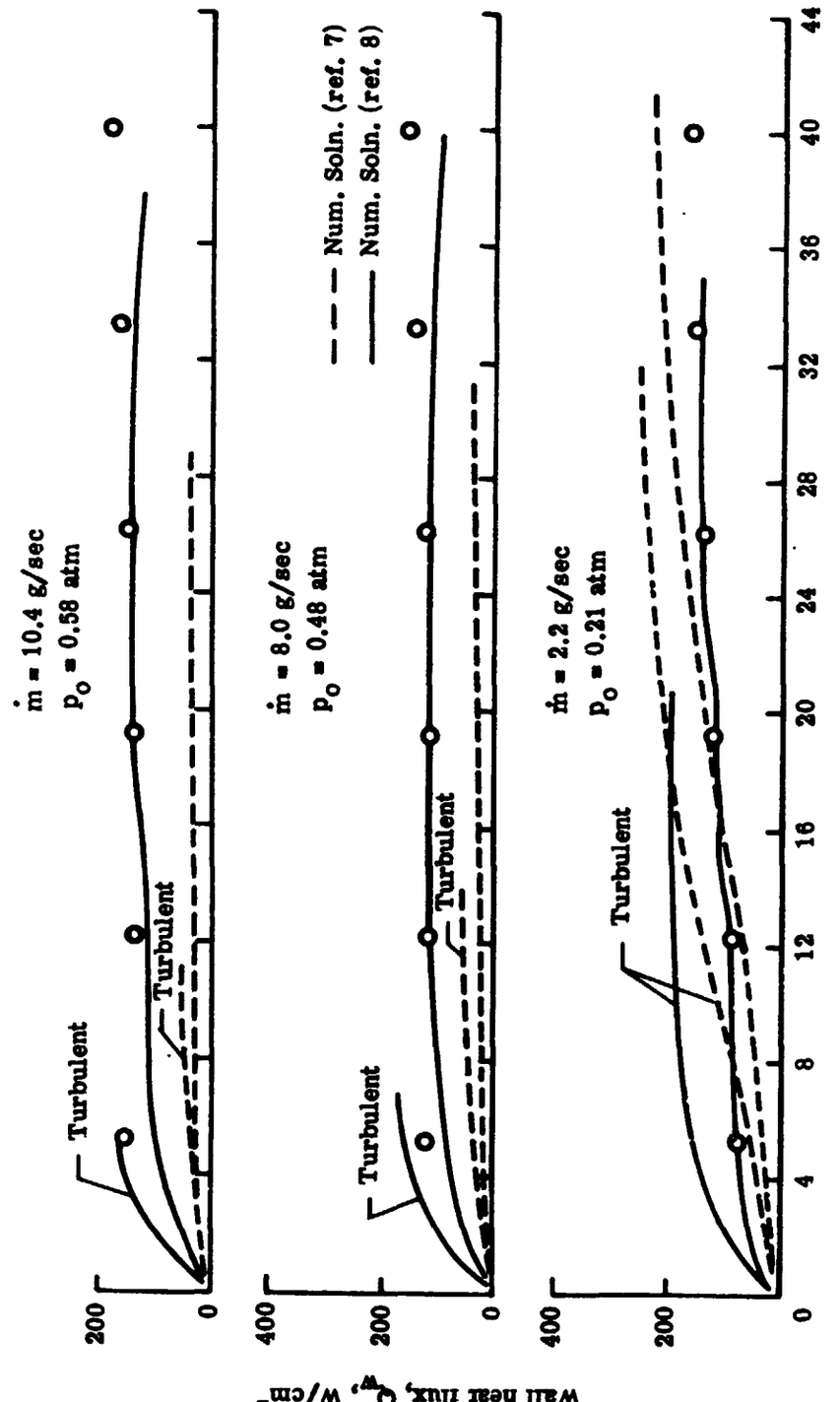

(c) Wall heat flux

Figure 6.- Continued.

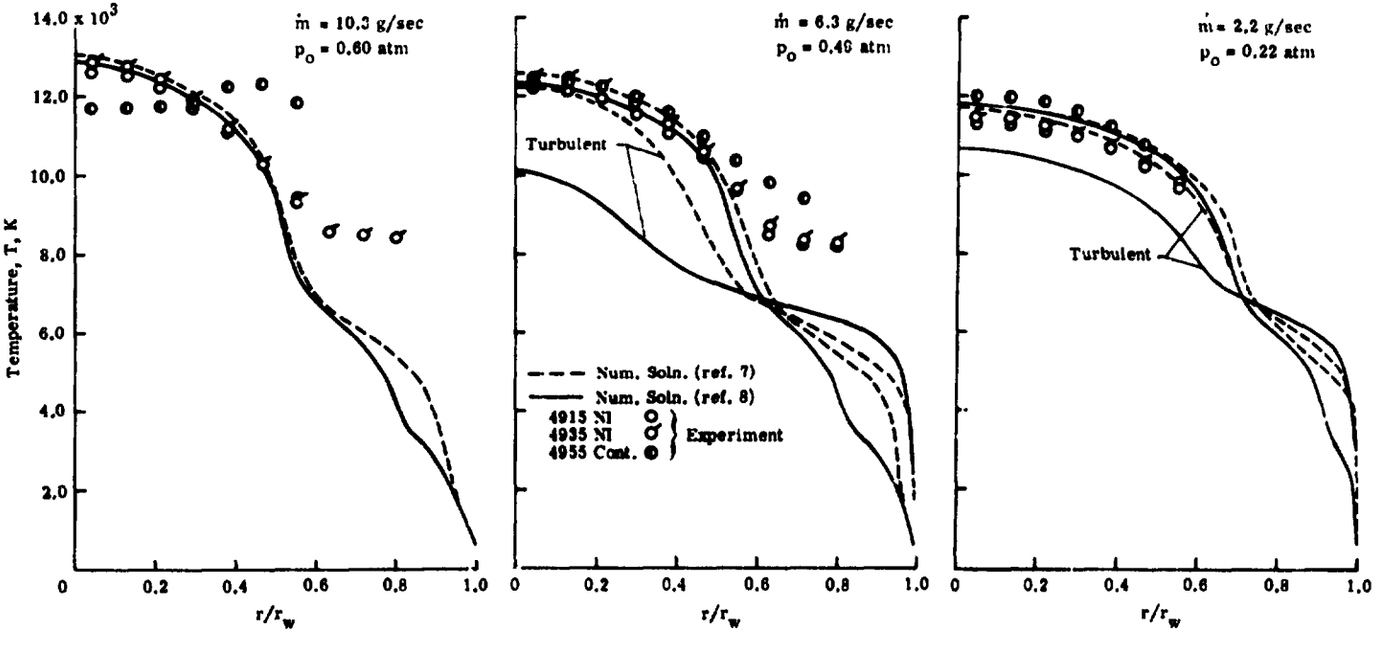

(d) Radial temperature profile at an axial location of z = 16.3 cm.

Figure 6.- Concluded.

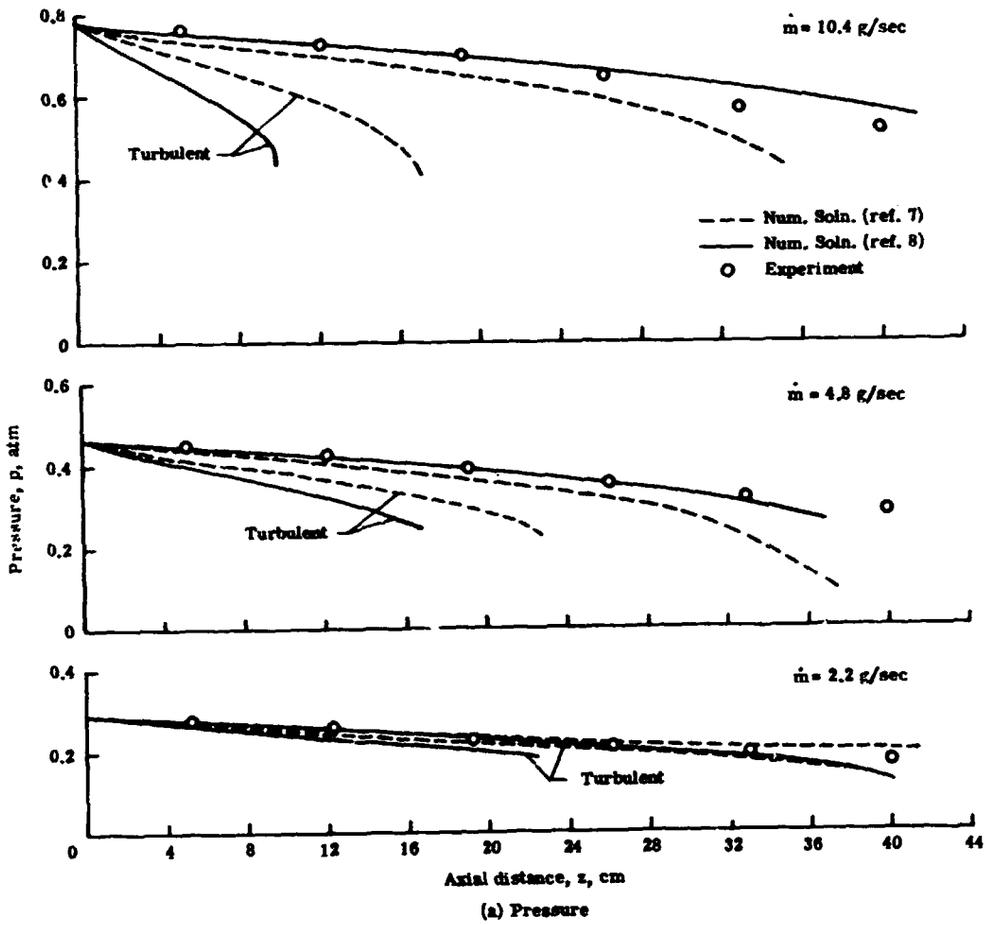

(a) Pressure

Figure 7.- Variation of parameters with axial location in the constrictor for I = 800 amps.

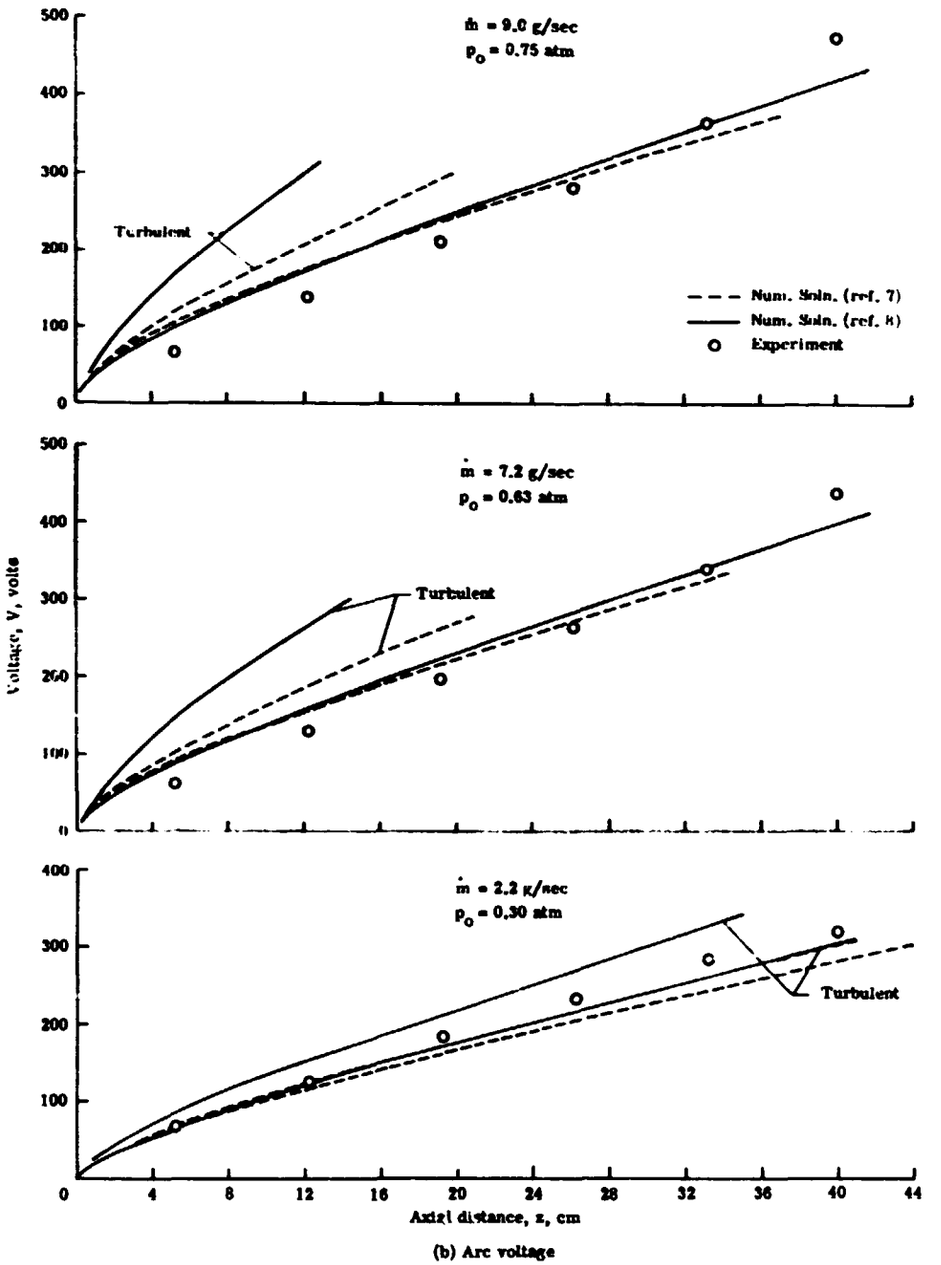

(b) Arc voltage

Figure 7.- Continued.

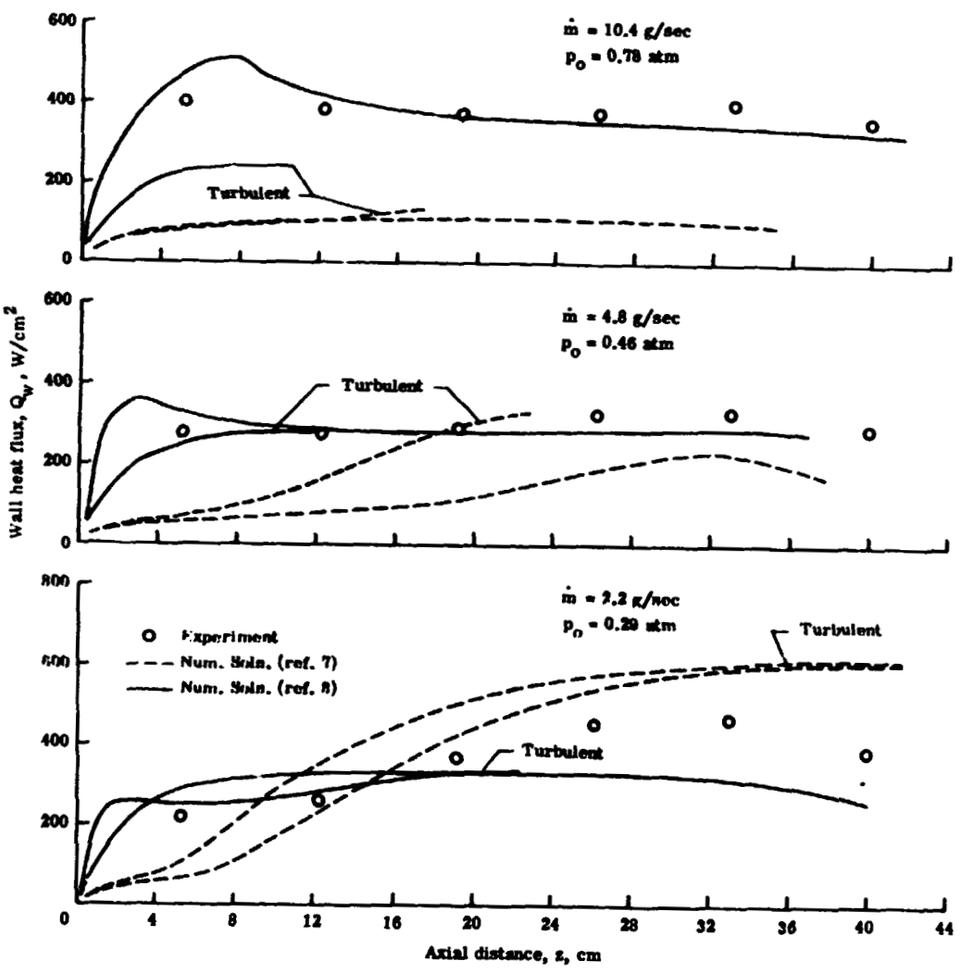

(c) Wall heat flux

Figure 7.- Continued.

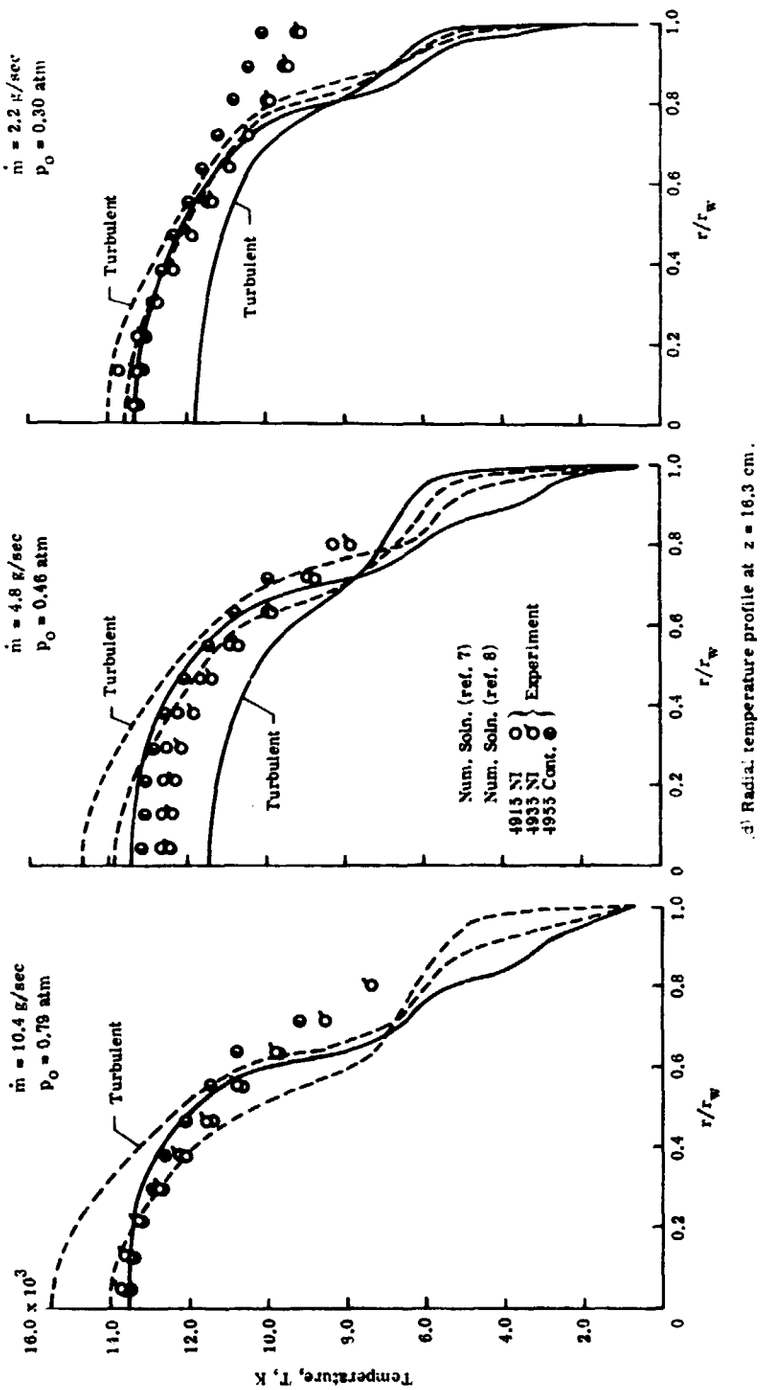

d) Radial temperature profile at z = 16.3 cm.

Figure 7.- Concluded.

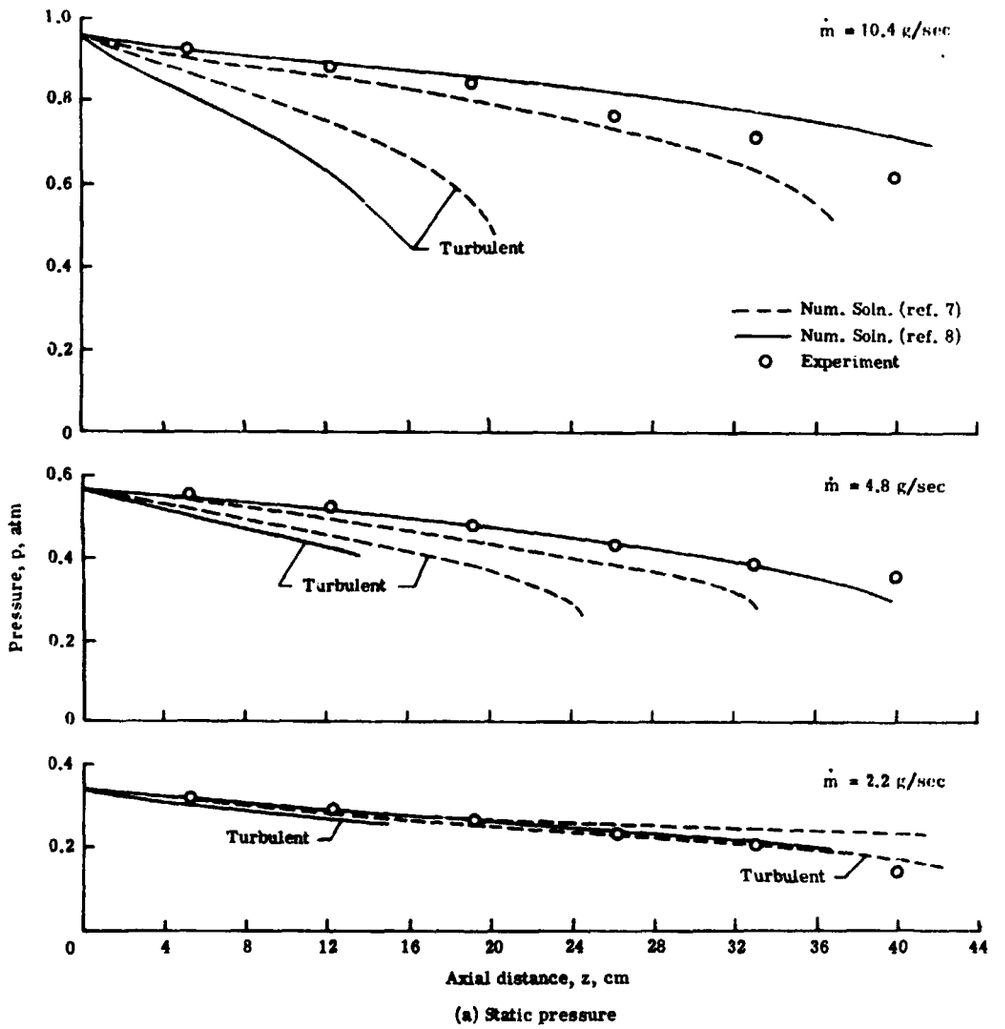

(a) Static pressure

Figure 8.- Variation of parameters with axial location in the constrictor for I ≈ 1200 amperes.

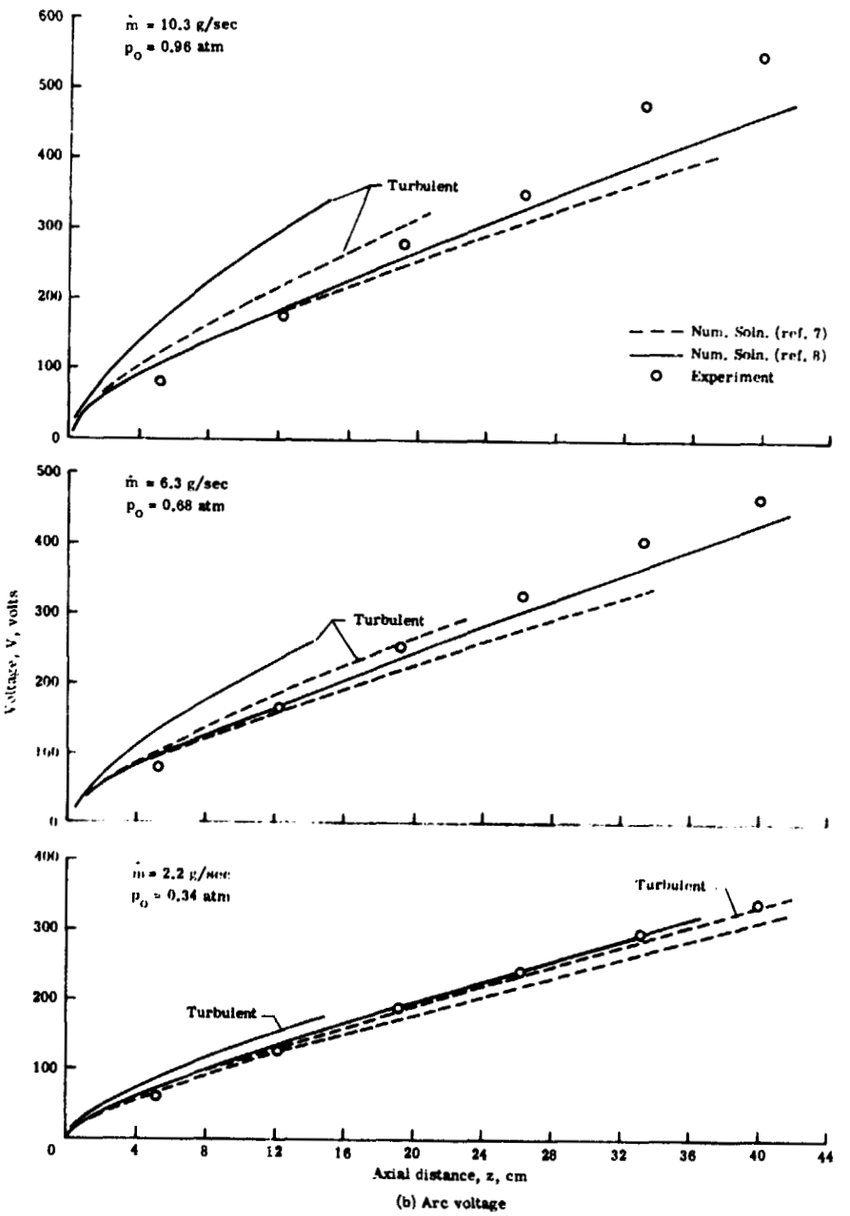

(b) Arc voltage

Figure 8.- Continued.

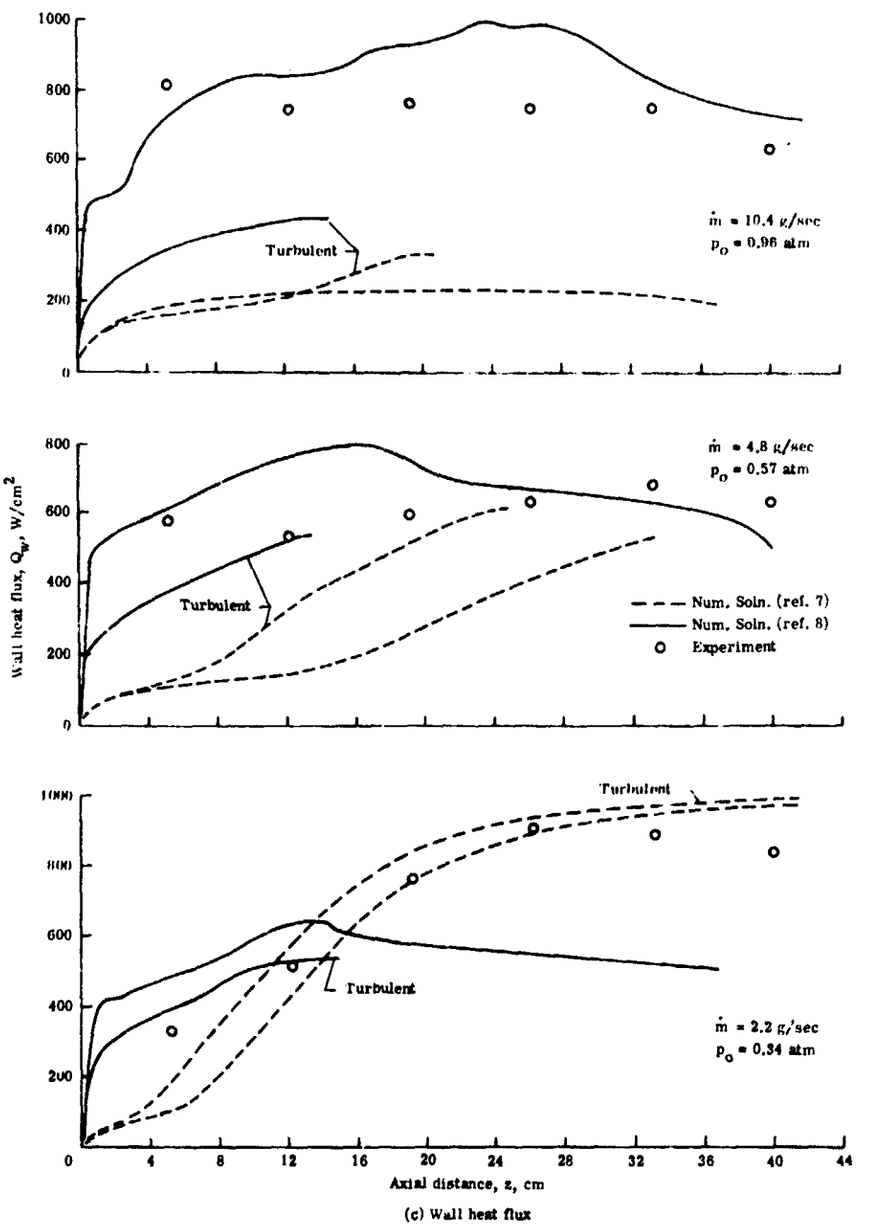

(c) Wall heat flux

Figure 8.- Continued.

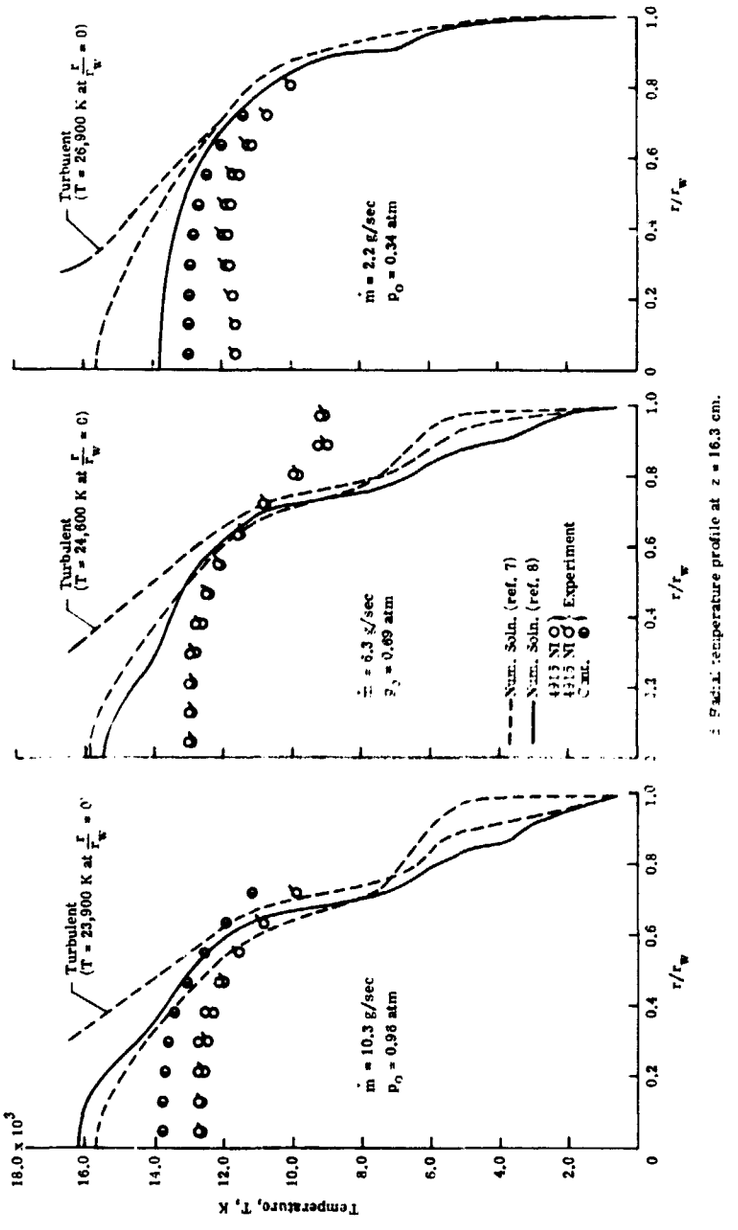

Figure 8.- Concluded.

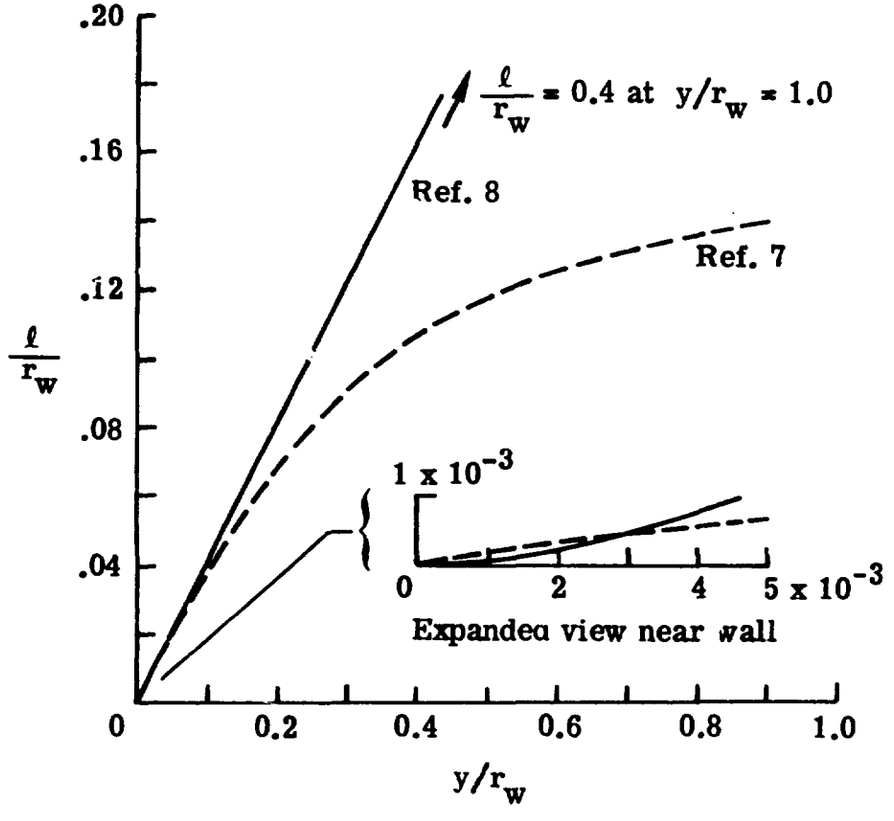

Figure 9.- Mixing length used in turbulent flow models of reference 7 and 8.

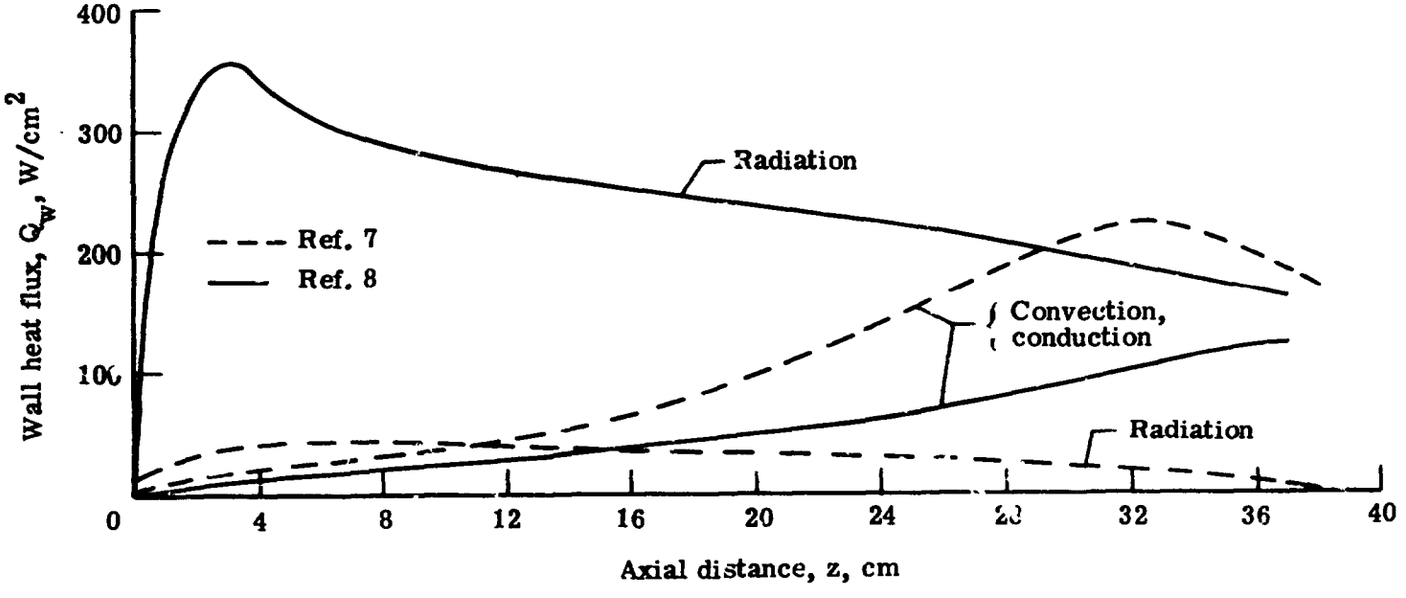

Figure 10.- Components of the total wall heat flux for reference 7 and reference 8. $I \approx 800$ amps, $\dot{m} = 4.8$ g/sec, $p_o = 0.46$ atm.

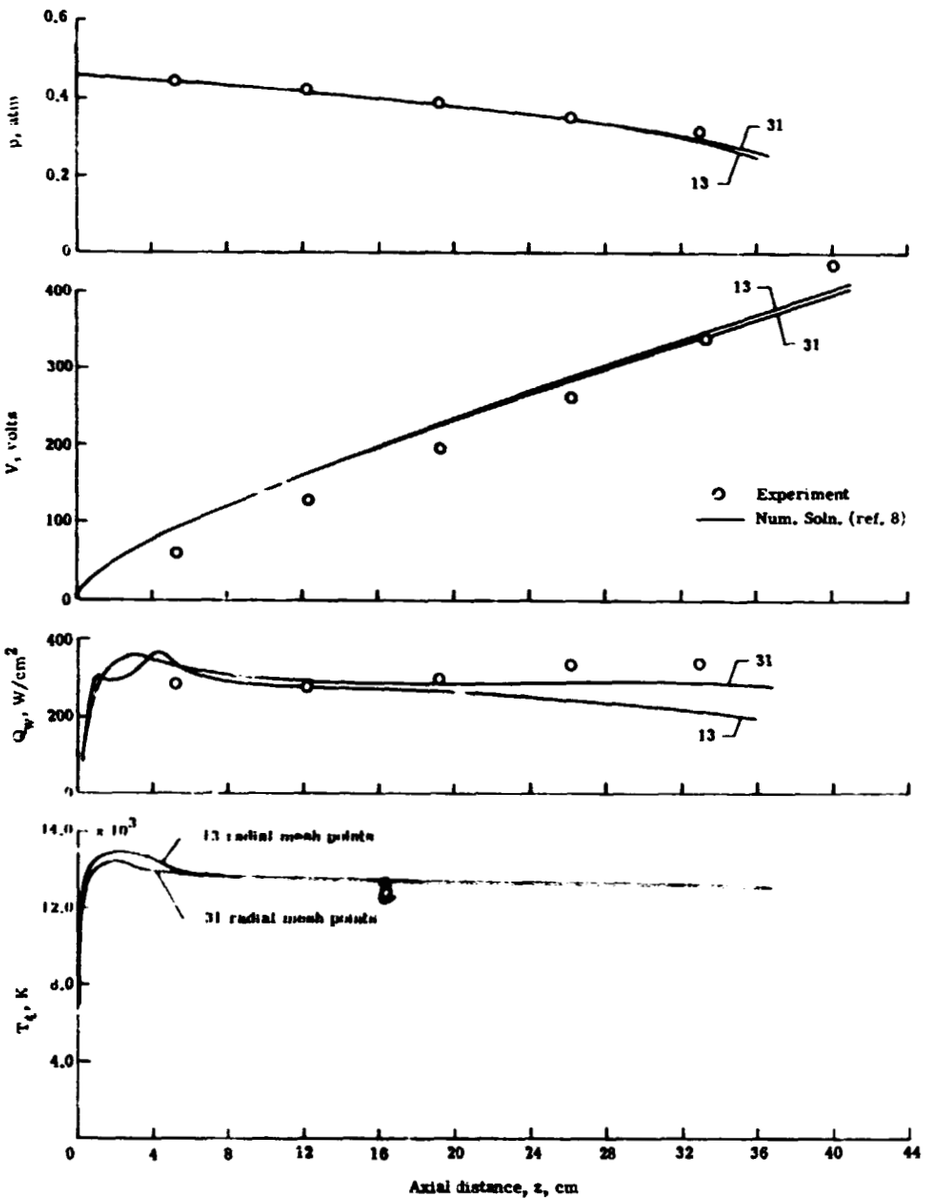

Figure 11.- Effect of number of radial mesh points on numerical solutions of reference 8. Laminar flow with I ≈ 800 amps, $\dot{m}$ = 5 g/sec, p_∞ = .46 atm.

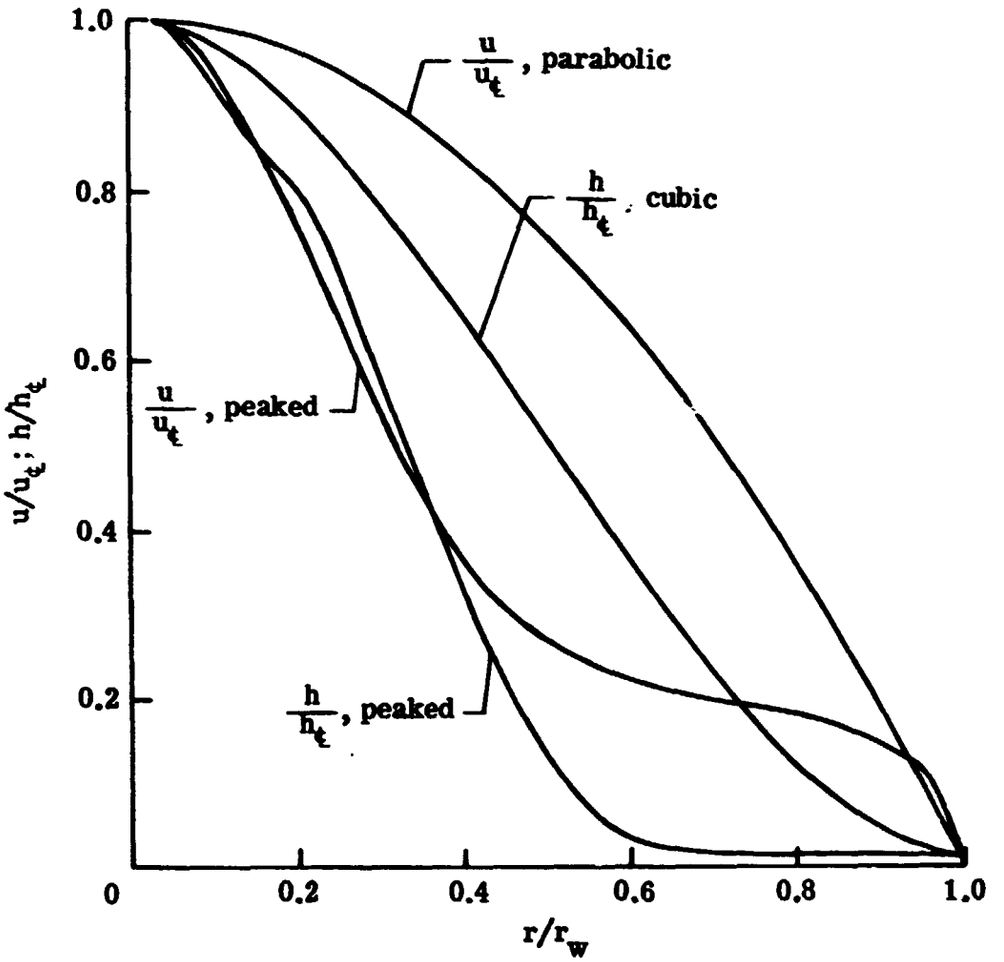

Figure 12.- Input entrance profiles of enthalpy and velocity for numerical solutions.

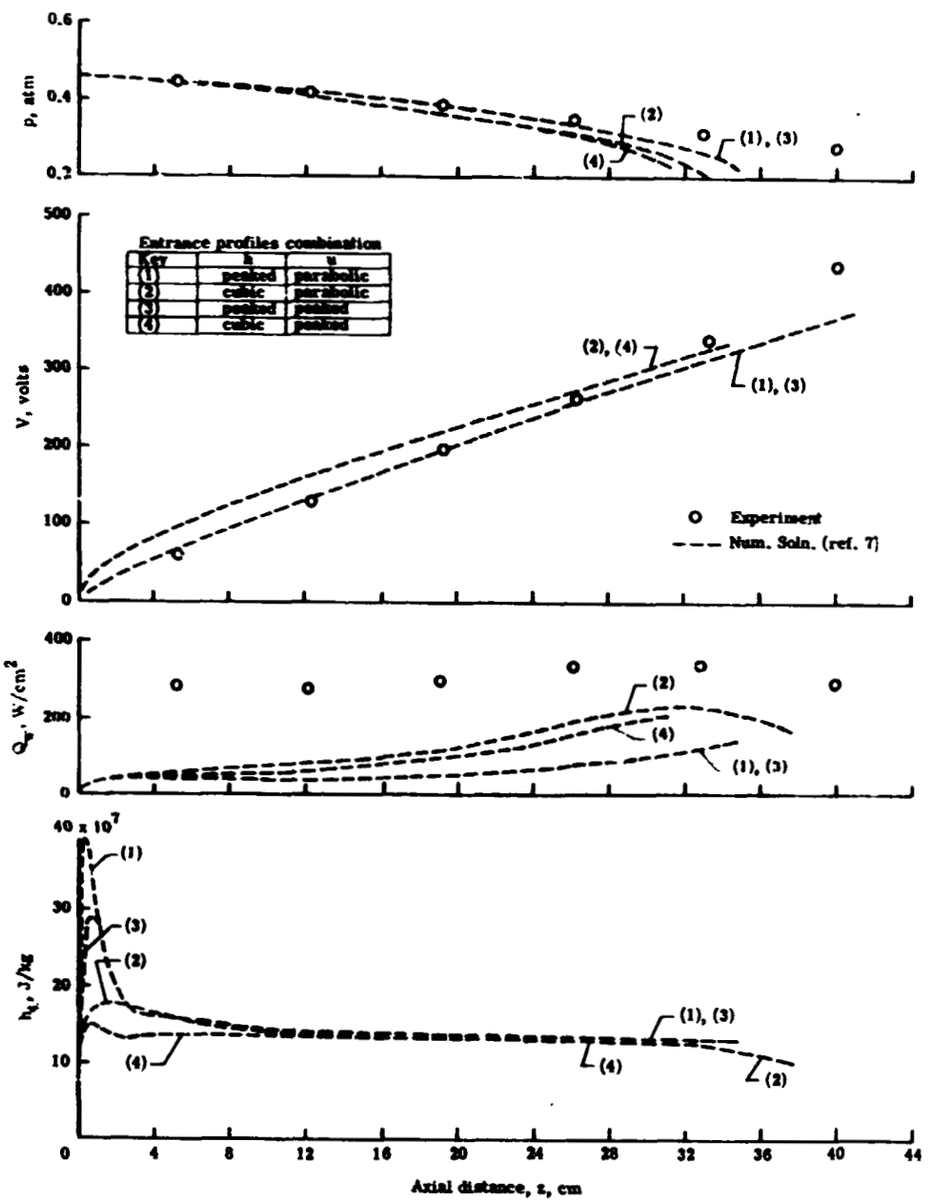

Figure 13.- Effect of entrance velocity and enthalpy profiles on numerical solutions of reference 7. Laminar flow with I ≈ 800 amps, $\dot{m}$ = 5 g/sec, p_o = .46 atm.

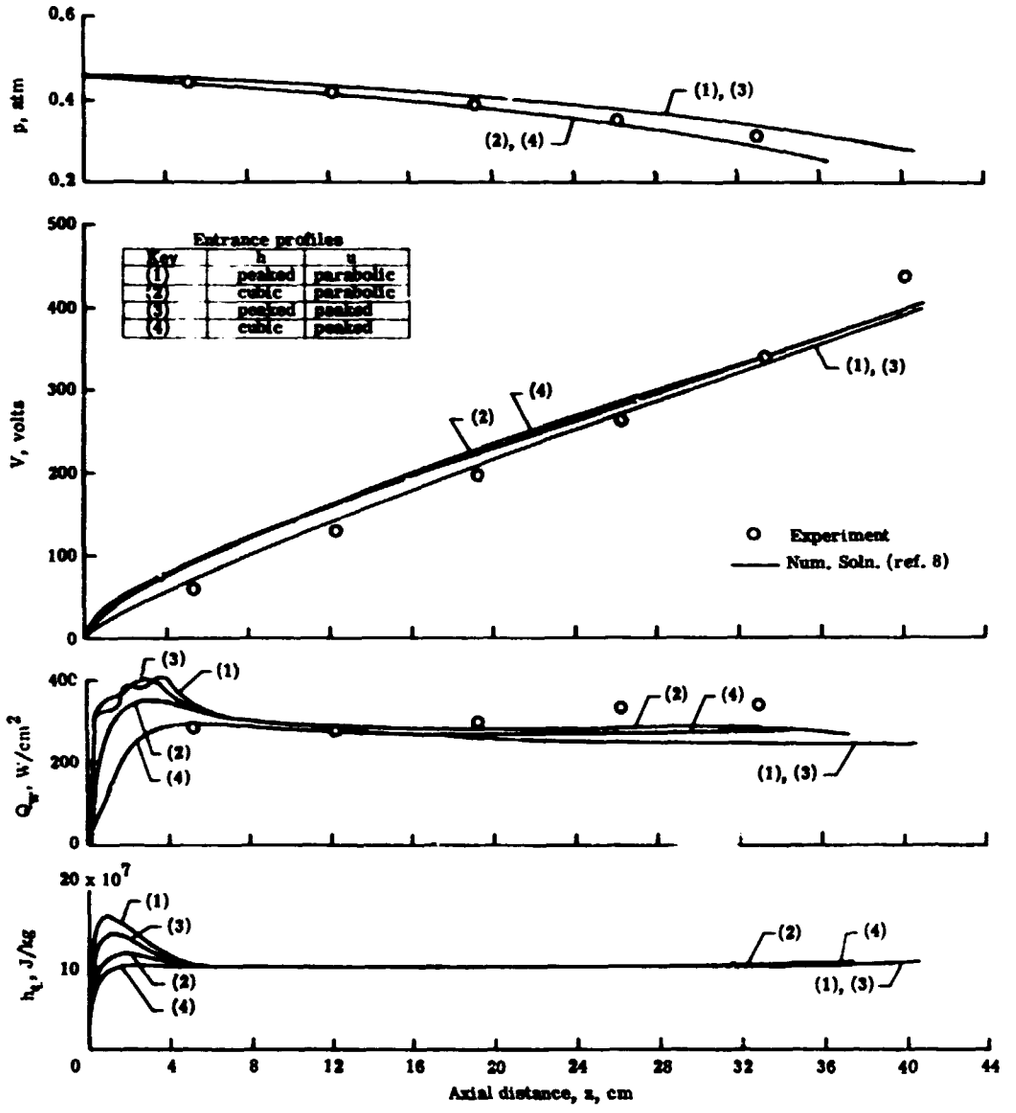

Figure 14.- Effect of entrance velocity and enthalpy profiles on numerical solutions of reference 8. Laminar flow with $I \approx 800$ amps, $\dot{m} = 5$ g/sec, $p_o = .46$ atm.